Journal of
Experimental and Theoretical Analyses

MDPI

Review

Review of Geosynthetic Encased Stone Columns for Mechanisms Modeling and Machine Learning Applications

Mohamed Abdellatief [1,*], Ayman ELtahrany [2] and Amr ElNemr [3]

[1] Department of Civil Engineering, Higher Future Institute of Engineering and Technology in Mansoura, Mansoura 35111, Egypt
[2] Department of Civil Engineering, Mansoura University, Mansoura 35111, Egypt
[3] Department of Civil Engineering, German University in Cairo, New Cairo 11835, Egypt; amr.elnemr@guc.edu.eg
* Correspondence: drmohamedabdellatief8@gmail.com

Abstract

Ground improvement for foundations supported on soft soils is traditionally problematic because of low bearing capacity and a large magnitude of settlement. One sustainable method for mitigating these problems is the use of stone columns (SCs), particularly geosynthetic-encased stone columns (GESCs), to improve load transfer, confinement, and consolidation. This review critically synthesizes recent advances in the analysis and design of SC systems using experimental investigations, numerical simulations, and machine learning (ML)-based methodologies. The article indicates that GESCs, when integrated with modern data-driven techniques, especially hybrid metaheuristic ML models, represent a reliable and sustainable solution for soft soil stabilization. Traditional analytical and empirical methods remain useful; however, they are often inadequate for very soft soils (Undrained shear strength (c_u) < 15 kPa), where excessive bulging and large deformations dominate system behavior. Consequently, intelligent hybrid modeling approaches are emerging as the next generation of optimized, data-driven design tools in geotechnical engineering. Different failure mechanisms of SCs, including bulging, punching shear, and general shear failure, are critically discussed along with the governing design parameters. Previous studies consistently indicate that spacing ratios within the range of $s/D = 2–3$ can improve the bearing capacity ratio (BCR) by approximately 50–100%. Numerical and experimental studies further demonstrate that SC systems can transfer nearly 60–80% of the applied load through stress concentration and soil arching mechanisms. Furthermore, the application of geosynthetic encasement enhances the performance of SCs in very soft soils by increasing confinement, reducing lateral deformation, and enhancing bearing capacity by nearly 3–6 times compared with ordinary SCs. The review also evaluates the growing role of artificial intelligence techniques in forecasting settlement and bearing capacity behavior. ML techniques such as artificial neural networks (ANN), support vector regression (SVR), random forest (RF), XGBoost, and hybrid metaheuristic–ML models have shown high predictive capability, often achieving prediction errors below 5%. Despite these advancements, many existing ML studies still suffer from limited datasets, a lack of generalization, and insufficient incorporation of physical mechanisms.

Keywords: stone columns; ground improvement; geosynthetic encasement; numerical modeling; machine learning; hybrid optimization

Academic Editor: Marco Rossi

Received: 8 April 2026
Revised: 4 June 2026
Accepted: 9 June 2026
Published: 18 June 2026

1. Introduction

Constructing stable foundations on weak or soft soils remains a major challenge for geotechnical engineering, as these soils have low bearing capacities, are compressible, and tend to exhibit high settlement [1,2]. Soft soils such as clays, silts, and organic deposits generally have low shear strength and consolidate under loading, threatening the stability of structures [3–5]. Many ground improvement techniques have been developed, including preloading [6], vertical drains [7], deep soil mixing [8,9], jet grouting [10], and vibro-replacement methods, including stone columns (SCs) [11,12]. SCs are widely used due to being economical, sustainable, providing additional strength and stiffness to the soil and reducing settlement [12–15]. SCs provide load transfer, increase bearing capacity, and expedite consolidation through drainage, providing the best solution for stabilization of soft soils [16–19] just by placing gravel-sized aggregate into the soil.

Stone columns, both encased and unencased, are a key technology in foundation engineering for providing an efficient means of supporting structures on difficult ground [16,19]. Uncased stone columns (also called ordinary stone columns (OSCs)) depend on the soil surrounding the column for lateral confinement, which can be limited in very soft silts or clays and cause buckling or shear failure [20]. Along with the stone columns, encasement, such as a geosynthetic or geotextile material, may help reduce this issue. Encased stone columns (ESCs) were created [16–19] to improve confinement, decrease lateral distortion, and increase load-carrying capacity. Because encasement materials such as geogrid [19] or geotextile [17] can provide columns with additional tensile strength, ESCs can work well in soils with an Undrained shear strength (c_u) as low as 5–15 kPa [13,14,16,19]. By using encasement, stone columns can be designed to work across a wider range of soil types, including organic and marine clays. Also, successful projects with ESCs include embankments [21–23], bridge abutments [23,24], and industrial foundations [25,26]. The use of SCs is multifunctional due to their adaptability across design variables such as column loading conditions and column configuration [25–28]. However, many of these studies have been largely case-specific or limited in scope, often failing to systematically quantify the combined influence of installation effects, long-term behavior, and encasement optimization across diverse site conditions. SCs remain an integral technology in modern geotechnical practice. Furthermore, in the case of long OSCs, when bulging failure occurs at the upper zones of the columns, the bearing capacity primarily relies on the confinement provided by the adjacent soft soil. Under very soft soils, OSCs generally will not provide much in terms of load capacity because of very low lateral confinement [29–31]. For this reason, the use of geosynthetics in the form of vertical encasing for additional confinement (VESC) or horizontal geosynthetic reinforcement layers (HRSC), is necessary [31].

Despite their common usage, the design and performance prediction of SCs is complex because of the numerous parameters, such as soil properties, column geometry, encasement stiffness, and loading. Experimental studies at varying scales (both small and large-scale laboratory studies and full-scale field tests) have yielded valuable information about load transfer mechanisms, failure modes ("bulging" or "punching" and "shear"), and installation methods [13,19,21,23]. Nevertheless, results from small-scale laboratory tests frequently overestimate performance due to scale effects and controlled boundary conditions, while full-scale field studies remain limited and highly variable. Analytical models provide relatively simple means of estimating bearing capacity and settlement, to a point, but do not adequately represent soil–structure interaction or related phenomena [19,27]. Numerical modeling, especially the finite element method (FEM) [27,32,33] and discrete element method (DEM) [34], has significantly improved understanding of SCs by allowing three-dimensional stress distributions and soil–column interaction under several conditions to be modeled [25,27,28]. While numerical methods such as FEM and DEM offer high-fidelity insights into the complex soil–column interactions and failure mechanisms, they are often computationally intensive and require extensive calibration of constitutive models. In contrast, ML models provide a faster, data-driven alternative capable of capturing nonlinear relationships and delivering rapid predictions of bearing capacity and settlement with high accuracy. This has led to the increasing adoption of ML techniques as complementary or alternative tools in the design and optimization of stone column systems [34–37].

In recent years, data-driven approaches, and in particular ML models, have emerged as powerful instruments for predicting SCs' behavior and optimizing design factors [38–40]. A variety of techniques have been employed, including artificial neural networks (ANN), support vector regression (SVR), random forests (RF), and extreme gradient boosting (XGBoost), to develop an understanding of the complex relationships between input variables such as soil strength, column geometry, and encasement properties, and output responses such as bearing capacity and settlement [41–44]. Also, hybrid metaheuristic-ML models, which utilize optimization techniques such as artificial bee colony (ABC) and harmony search (HS), have demonstrated high accuracy in bearing capacity estimation (R^2 values of 0.981–0.989 for ABC and 0.984–0.988 for HS) [40]. Despite these promising results, most ML studies rely on limited or synthetic datasets and rarely integrate physical mechanisms, limiting their practical reliability and generalizability. Furthermore, these intelligent methods utilize limited datasets with rapid, accurate predictions that would minimize resource dependence on costly experimental and numerical analyses [35,40]. Previous review papers offered good summaries of SC behavior based principally on experimental and numerical work. However, they generally lacked a truly integrative perspective on emerging ML techniques and failed to critically evaluate the practical limitations and inconsistencies across studies [45–47]. They often neglect more advanced and time-dependent behaviors (e.g., creep and consolidation), standardization of encasement parameters, and the sustainability assessment of SC designs. Moreover, the scarcity of open-access datasets further restricts the development and validation of robust AI models [48–50].

2. Synthesis Method and Decision Framework

To ensure a transparent, reproducible, and comprehensive synthesis of the literature, a structured methodology was developed and adopted. Following the systematic literature search (Scopus, Web of Science, and Google Scholar databases using keywords such as "stone column," "geosynthetic encased stone column," "bearing capacity," "settlement," "machine learning," and "failure mechanism" for publications between 2010 and 2026), studies were screened using clear inclusion and exclusion criteria based on relevance, methodological quality, and contribution to experimental, numerical, or ML aspects of stone column performance. This process followed the PRISMA 2020 guidelines [51] and resulted in the selection of more than 162 references. The study selection process is illustrated in Figure 1. A hierarchical decision framework was then applied to categorize the selected studies into three main streams: experimental investigations, numerical simulations (FEM/DEM), and machine learning (ML)-based studies. Quality assessment criteria included methodological robustness, clarity of reported results, adequacy of sample size or dataset, validation approaches, and practical relevance to geotechnical applications. This framework enabled a balanced, critical synthesis across the different research approaches, while identifying synergies and gaps.

https://doi.org/10.3390/jeta4020022

This review provides a thorough synthesis of the current state of the art in stone column (SC) research, covering both ordinary stone columns (OSCs) and geosynthetic-encased stone columns (GESCs). It integrates findings from experimental, analytical, numerical, and machine learning (ML)-based studies to elucidate the key factors governing SC performance under varying soil conditions and loading scenarios, as illustrated in Figure 2. The review subsequently examines recent advances in data-driven modeling, with particular emphasis on hybrid metaheuristic algorithms for bearing capacity prediction and outlines future directions for hybrid physics-informed AI models. Additionally, it identifies critical gaps in the existing literature, including limited integration between numerical and ML frameworks, and the scarcity of publicly available high-quality datasets from field and experimental investigations. By addressing these gaps, the review aims to guide future research toward more sustainable and efficient ground improvement solutions in geotechnical engineering.

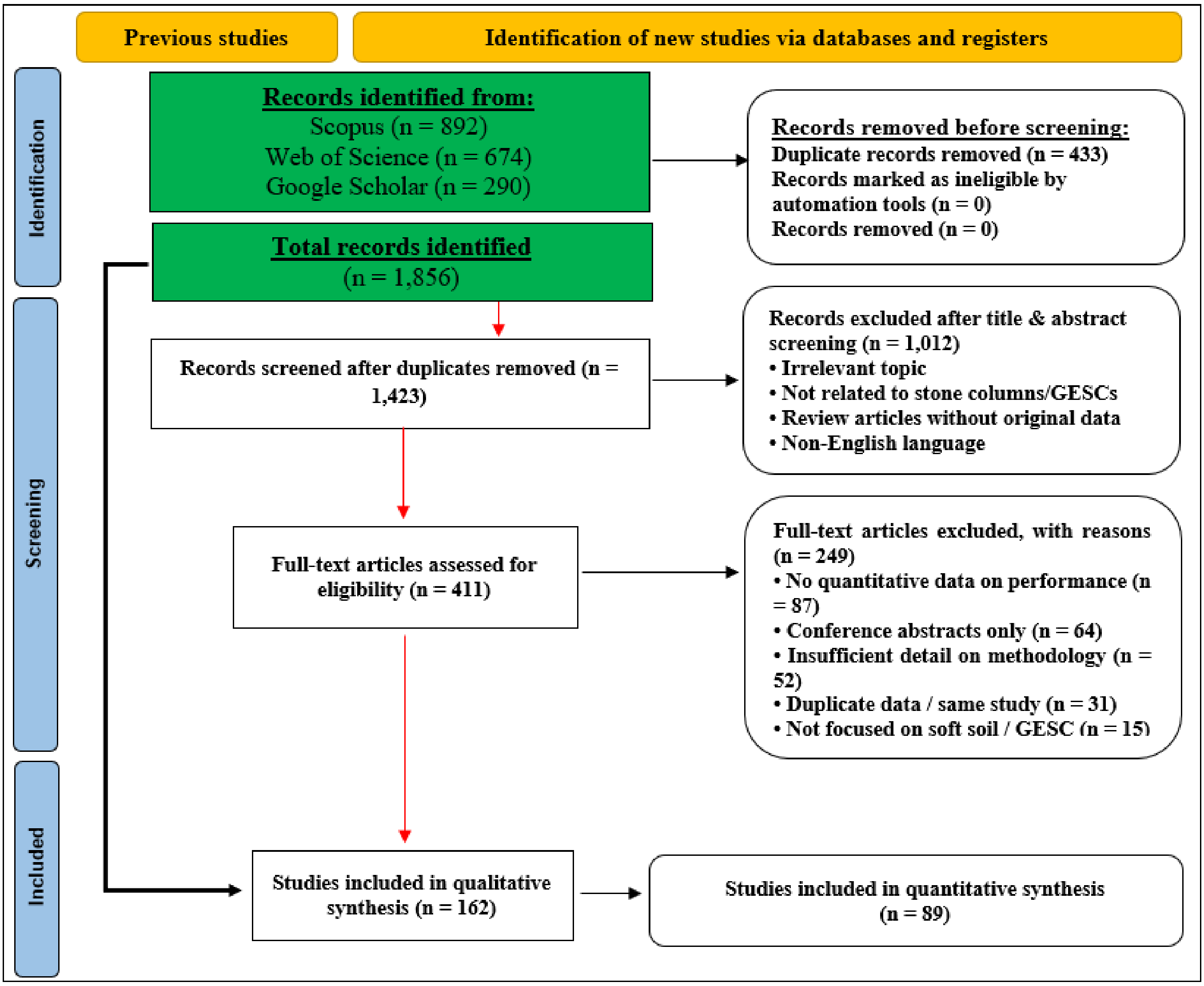

Figure 1. PRISMA flow diagram of the systematic review process [51].

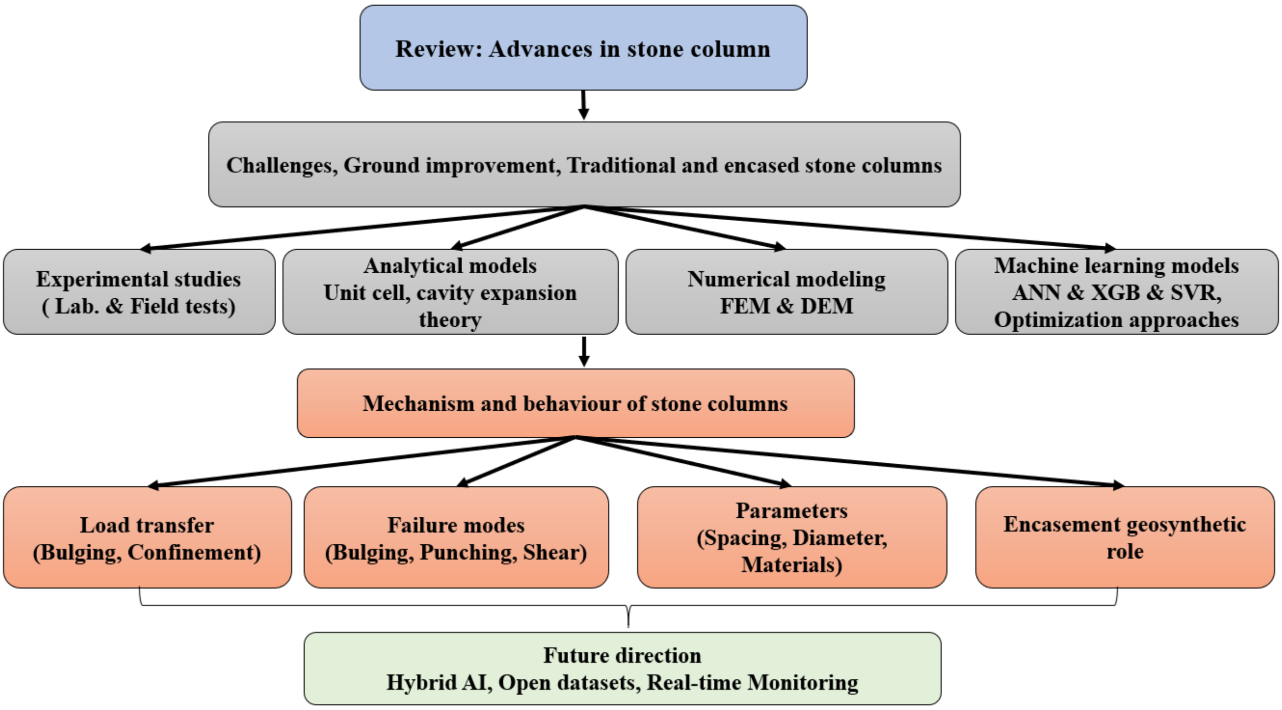

Figure 2. Integrated conceptual framework explaining the overall research structure adopted in this review.

3. Mechanism and Behavior of SCs

This section explores the basic mechanisms controlling SCs' behavior, drawing on experimental findings, numerical analysis, and recent investigations. It describes the mechanics of load transfer, failure modes, sensitivity to parameters, and the encasement effect, laying the groundwork for predictive modeling to be discussed in the next section.

3.1. Basic Working Principles

SCs work by replacing the weak soil with high-strength granular material, which can be a more effective way to redistribute loads in soft ground. The main working principle is vertical load transfer. When vertical loads are applied by the overlying structure, the applied stresses are, in essence, carried mainly by the stiffer column material, which has a high deformation modulus. For example, stone aggregates have a deformation modulus of 50–200 MPa, compared to the surrounding soft clays or silts, which range from 1–10 MPa [29,50,52]. As the column is loaded, it is axially compressed, and radial stresses are activated, resulting in soil arching within the surrounding soil matrix. This soil arching redistributes the applied load, thereby increasing the composite stiffness of the improved ground system [48–50]. Vertical stress concentrations in the column core and shear resistance along the column-soil interface are how the applied load is transferred from the column to the soil [48,53,54].

Finite element studies [22,34,41,49,55] have found that roughly 60–80% of the load applied is transmitted vertically through the stone column, and 20–40% is transferred through interfacial friction and arching in the surrounding soil situation, given that the column is working in composite action. The resulting composite action reduces the time it takes for pore water to dissipate and reduces overall consolidation and settlement by 50–80% in soft clay foundations [53,56,57]. Thus, this effect is quantified through the stress concentration ratio (*SCR*), which is the average vertical stress in the SC (σ_c) relative to the average vertical stress in the surrounding soil (σ_s) and is defined as:

$$SCR = n = \frac{\sigma_c}{\sigma_s} \quad (1)$$

Typical field observations and numerical back analyses indicate SCR values ranging from 2.5 to 5.0, based on column spacing, rigidity contrast, and installation procedure [58–63]. Larger n or SCR results in better performance of the overall foundation and less settlement of the soil because of a more efficient load transfer to the column. In addition, the consolidation settlement reduction ratio (R_s) can be calculated using the area replacement ratio (a_s = A_c/A), where A_c is the cross-sectional area of the stone column, and A is the tributary area of soil, as follows [58]:

$$R_s = \frac{1}{1 + (n-1)a_s} \quad (2)$$

This relationship suggests that a combination of column stiffness and geometry (spacing and diameter) plays a major role in the settlement response. Parametric studies in the literature conducted during numerical studies with 3D FEM [58,61,62] revealed that increasing the area replacement ratio from 10% to 25% (related to the cross-sectional area of the columns) can potentially, when compared to field measurements, generate an approximately 70% reduction in settlements.

Bulging is a form of deformation that occurs when a column is subjected to axial load and is defined as the column's outward expansion, especially in very soft soils c_u < 15 kPa). This deformation occurs at depths of roughly 2–4 diameters below the top of the column and is attributed to Poisson's effect and insufficient lateral support. Findings from recent DEM simulations [34,57] demonstrated that bulging depth is dependent upon particle size (D_{50} > 20 mm), yielding effective lengths that are reduced by 20–30%. If the column is not restrained, bulging limits bearing capacity to values between 200–400 kPa [53,58,63].

Confinement is essential for maintaining both the stability and load-carrying capacity of SCs. It can be provided by the shear strength of the surrounding soil or by external geosynthetic encasement. For columns without encasement, the lateral confining stress,

$$\boldsymbol{\sigma}_h = \mathbf{k}_0 \boldsymbol{\sigma}_v + 2c_u \quad (3)$$

where $\boldsymbol{\sigma}_h$ is horizontal stress; $\mathbf{K}_0$ is the coefficient of lateral earth pressure and typically ranges from 0.5 to 1.0; and $\boldsymbol{\sigma}_v$ is vertical stress. If soil is adequately confined, it will not deform excessively, and vertical stresses will be redistributed by the unit cell in which the stone columns reside, equivalent to a cylindrical zone of influence with an area of $\pi s^2/4$, where s is column spacing [64–66].

Experimental studies have demonstrated that higher confinement ratios (typically > 1.5) can increase the bearing capacity of stone columns by a factor of 2–3 under ideal laboratory conditions [64–66]. However, the practical significance of lateral restraint must be interpreted cautiously, as these gains are often highly sensitive to soil undrained shear strength, installation quality, and loading conditions. The key principles of confinement and their implications for column behavior are summarized in Table 1. The load transfer mechanisms in stone columns have been extensively corroborated by both experimental and numerical investigations, including those by Zhang et al. [66]. A stiffer column typically attracts a larger share of the applied load, resulting in higher vertical stress concentration (α_c) within the column and lower stress (α_s) in the surrounding soil. This stress differential induces radial bulging, which is effectively resisted by the lateral confinement provided by the surrounding soil or geosynthetic encasement. While geosynthetic encasement significantly enhances soil arching and load redistribution, transferring approximately 60–80% of the applied load to the column, several studies highlight important limitations. In very soft soils (c_u < 15 kPa), the effectiveness of confinement can diminish over time due to creep, clogging, or insufficient encasement stiffness, leading to reduced long-term performance. Consequently, although geosynthetic-encased stone columns consistently achieve improved composite stiffness and lower total settlements in controlled laboratory and finite element analyses, field observations frequently indicate greater variability and lower improvement ratios than those reported in idealized numerical simulations.

Table 1. Key principles and parametric influences on SC behavior.

Parameter	Description	Typical Range/Effect	Ref.
Load transfer (SCR, n)	Stress concentration ratio σ_c/σ_s is governed by arching and interface friction between the column and the surrounding soil.	2.5–5.0; higher n = 50–80% reduction in settlement	[58]
Area replacement ratio (a_s)	A_c/A ratio; higher a_s it improves composite stiffness and load sharing.	10–25%; up to 70% reduction in settlement	[64–66]
Bulging depth	Depth of maximum lateral expansion (=2–4D from top of column)	D_{50} > 20 mm achieve 20–30% increase in bulging depth	[67–70]
Confinement	$\sigma_h = k_0\sigma_v + 2c_u$; higher confinement ratio enhances stability	Confinement ratio > 1.5 achieve 2–3 times increase in bearing capacity	[29,70,71]
Clogging	Migration of fine particles at the soil–aggregate interface reduces drainage	30–50% decrease in permeability over time	[72,73]
Barreling Effect	End-restraint–induced lateral expansion of the column during loading	15–25% increase in lateral strain	[74,75]
Consolidation	Rate of pore pressure dissipation as per Equation (2) [58]	50–80% reduction in consolidation time and settlement	[74–77]
Encasement	Geogrid-induced confinement provides tensile restraint and improved load transfer	2–4 times increase in capacity; achieve 40% reduction in bulging	[77–79]

3.2. Failure Modes

Failure in SCs arises from soil–column interaction under monotonic or cyclic loads, classified into three modes based on geometry and soil strength.

Bulging failure dominates in medium-soft soils (c_u = 15–25 kPa), where the column deforms outward like a bellows, forming a "barrel" shape. Laboratory experiments suggest that the maximum bulge usually occurs on or about the midpoint of the column at a corresponding failure load of $q_f = 4c_u(D/L)^{0.5}$. FEM analyses using the Mohr–Coulomb model verified these claims and revealed an approximate reduction in load capacity of 30–50% without confinement or mitigation measures [60,80].

Punching failure occurs in very soft soils (c_u <10 kPa) or end-bearing columns, where the column penetrates the surrounding soil vertically, akin to a pile. It features minimal lateral spread, with settlement > 10% diameter [81–84].

Shear failure affects groups or deep layers, involving sliding along the composite mass. It combines general shear (soil failure planes at 45° + $\varphi/2$) and column shear ($\tau_f = c + \sigma \tan\delta$), where δ is the interface friction angle. In field studies of marine clay deposits, shear failure is primarily observed in arranged column groups at larger spacing ratios (s > 3D), where the BCR is usually less than 2.0. More recently, a metastudy presents that hybrid failure modes, where both bulging and punching occur, are observed in just under 60% of all published cases. Figure 3 presents the failure mechanisms, while Table 2 summarizes comparisons of key features and factors that may be related to consideration of the mechanisms [85–88].

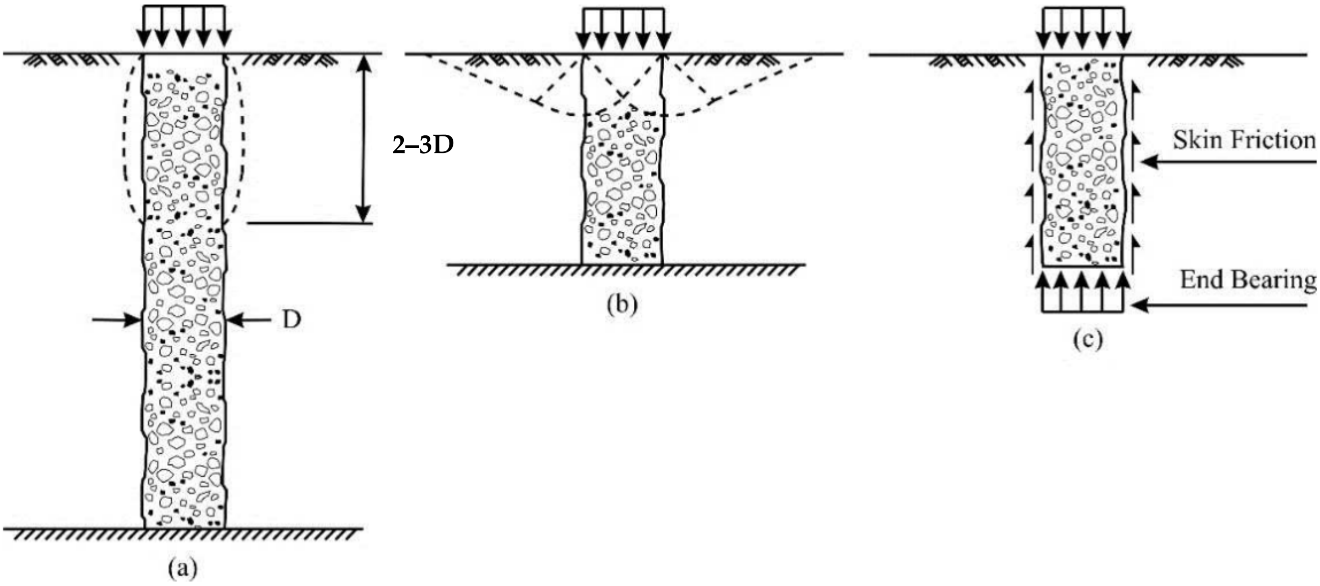

Figure 3. Failure modes of individual columns: (**a**) bulging failure, (**b**) shear failure, and (**c**) punching failure [87,88].

Table 2. Comparison of failure modes and prediction methods.

Method	c_u (kPa)	Geometry (L/D, s/D)	Bearing Capacity	Key Equation/Effect	References
Bulging	15–25	L/D > 5; s < 3D	Bearing capacity = $4c_u (D/L)^{0.5}$; BCR = 4–6	30–50% capacity loss without confinement	[60,76,85]
Punching	<10	L/D < 5; end-bearing	BCR = 2–3; 40–60% lower than bulging	Settlement > 10%D at failure	[81,82]
Shear	>25	s > 3D; column groups	BCR < 2.0; $\tau_f = c + \sigma \tan \delta$	Hybrid (bulging + punching) in 60% of cases	[80–82,86]
All	-	Any arrangement	Lower-bound bearing capacity	3D analytical solution for composite ground	[83]

where L—Length of stone column (m), s—Center-to-center spacing between columns (m), τ_f—Shear strength at failure (kPa), c—Cohesion of soil (kPa), σ—Normal stress (kPa), and δ—Interface friction angle (°).

Kang et al. [80] introduced the method of overlap to supplant traditional welding processes to address challenges presented by the welding frames during field construction of GESCs (Figure 4). This method has the advantages of simplicity and cost savings by installing an encasement in the field; however, the bearing mechanism needed clarification. Through conducting compression tests on multi-layer GESCs under dynamic loading and static loading, it was demonstrated in this study that the column modulus and lateral confinement are increased with the number of encasement layers. The enhancement in stress transfer and decrease in internal damage can be attributed to the corresponding increase in vertical ultimate bearing capacity, which can be as large as a difference of 47.1% between dynamic and static loading conditions. The location of the main radial strain does not change with loading type; however, dynamic loading tends to reduce lateral restraint, decreasing stress transfer efficiency and resulting in a smaller radial strain, most uniformly distributed across the height of the columns. The effects of considering cyclic or traffic-induced loads in GESC in foundation design and optimizing the number of encasement layers were supported through this study to improve the performance of GESCs in soft ground improvement applications.

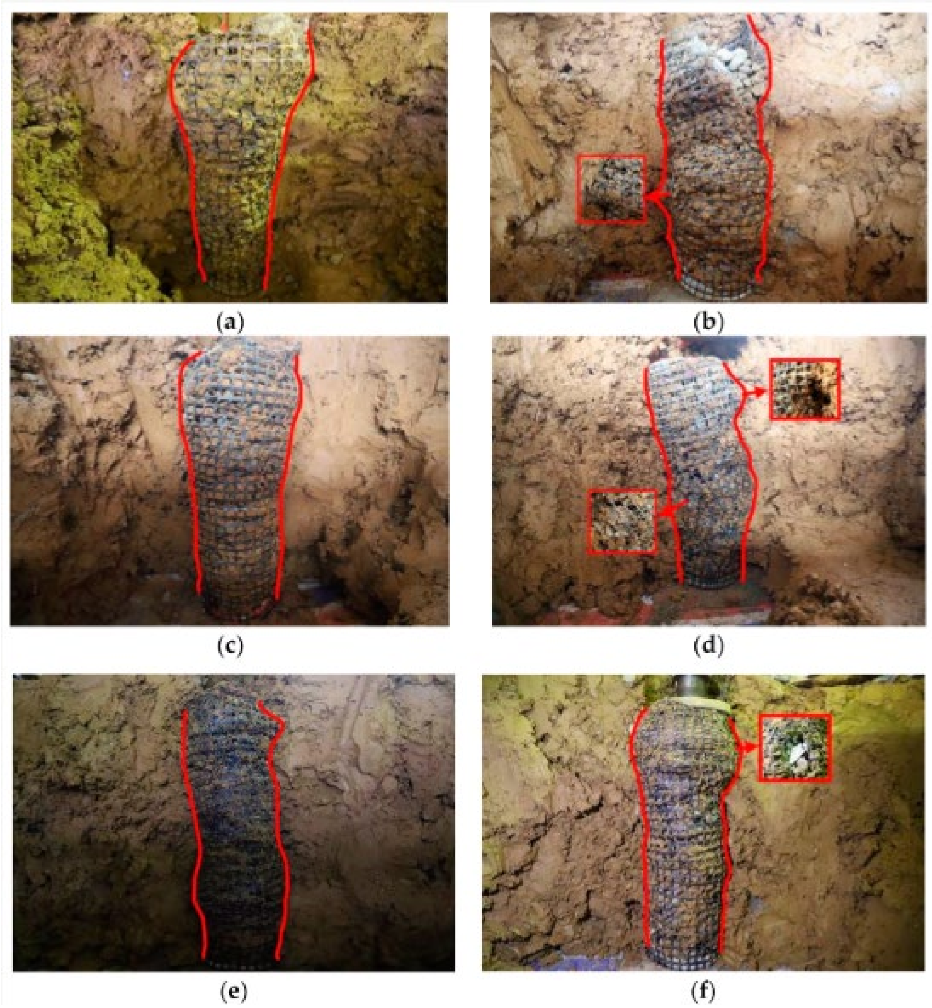

Figure 4. Failure modes of GESCs during dynamic and static loading. Failure Modes: (**a**) S1, (**b**) D1, (**c**) S2, (**d**) D2, (**e**) S3, and (**f**) D3 [80].

3.3. Influence of Parameters

SC performance is critically determined by variations in parameters, supported by earlier parametric FEM/DEM studies [67,71,74,75]. These parameters interact with installation effects, or strains of the soil state due to installation (e.g., increasing pore pressures, increases in horizontal effective stresses, and the effect of remolding), which are overlooked in design but offer information and enhance the reduction in settlement in soft cohesive soils [52,60,69]. The availability of installation effects in construction through cavity expansion (2 to 8%) or enhanced stiffness zones can increase the overall BCR from 5 to 40% beyond the geometric factors' effects.

Column spacing (s): Spacing between columns controls the efficiency of the group and the arching effect. Closer spacing (s/D = 2–3) improves the overlap of axial and lateral stresses (Table 3), thereby improving the BCR by 1.5 to 2.0. When spacing exceeds s/D = 4, the interaction becomes minimal and behaves similarly to a single isolated column (BCR = 1.5). Effects of installation contribute to the above; for example, field data presented a reduction in settlement of about 20% s = 2.5D due to the remolded areas around the columns [83]. Previous studies [84,89,90] of numerical sensitivity also indicated a 10% reduction in s increases to bearing capacity of the soil by 12 to 18% in addition to volumetric strain field conditions.

Diameter (D) has a significant influence on the bearing capacity of SCs. The ultimate bearing capacity generally increases with column diameter, often following a relationship proportional to $D^{0.5–1.0}$, depending on the failure mechanism and soil conditions. Increasing the column diameter from 0.8 m to 1.2 m typically results in a 30% to 50% increase in the BCR due to a larger friction area and improved load distribution. However, larger diameters also lead to exponentially higher volumes of backfill material and greater installation disturbance (remolding) in cohesive soils [83,91,92]. Parametric studies [76,77,84] indicate that a 10% increase in diameter can enhance ultimate bearing capacity by up to 15%. On the other hand, installation-induced mean stress increases may cause an 8–15% reduction in capacity under high loading conditions [62,67,73].

Material type influences friction, drainage, and interactions with installation effects. Crushed aggregate (φ = 40–45°) outperforms gravel (φ = 35–40°), with 25% high modulus and perfect cavity stability. Recycled materials produce a −20% cost and φ = 5° lower than gravel, slightly counteracting the installation densification benefits associated with transitional soils [48,53,54,56]. Gravel permeability improves the rate of consolidation and stabilization of pure cohesive clays by 20 to 30% compared with ungravelled soils [93]. Figure 5 gives a comprehensive picture of the response of both reinforced and unreinforced clay under loading conditions. Figure 5a explains that lateral deformation decreases with depth, with the maximum occurring at roughly 5 m, and demonstrates that crushed aggregate columns (CAC) are more effective in reducing deformation compared with scoria gravel columns (SGC). Figure 5b shows that the greatest horizontal deformation occurs at the center of the loaded area, and with increased offset, the horizontal deformation diminishes.

In addition, CAC also demonstrated greater immobilization of clay than SGC, consistent with Figure 5a. Figure 5c presents the numerical results compared with Dogan and Kahyaoglu [94], Debbabi et al. [95], and Shivashankar et al. [96], all of which present similar deformation patterns to Negesa [93], who has confirmed that the maximum bulging occurs at roughly one-third the depth from the surface to the end of the column.

Table 3. Parameters' effects on BCR and settlement.

Parameter	Range	BCR Gain (%)	Settlement Reduction (%)	Installation Synergy	Source
Spacing (s/D)	2–3	50–100	20–35	+12% (due to remolding and lateral stress increase)	[92]
	>4	0–10	5–10	+5%	[48,91]
Diameter (D)	0.6–0.9	30–50	15–25	+8–15% (stress rise)	[84,90,94]
	0.8–1.2	40–60	20–30	+10% (void control)	[81,82,85]
Material (φ, °)	Gravel (35–40)	Baseline	10–20	+20% drainage	[53,54,57]
	Crushed (40–45)	+25	15–25	+25% modulus	[83,84,87,89,90,94]

Installation effects integration: In addition to geometric parameters, the process of cavity expansion that occurs during vibro-installation increases lateral earth pressure (K_0 by 20–50%) and stiffness (up to 2 times initial) of the soil in 1.5-like to up to 2D zone [96,97]. Consequently, this results in a 5–25% decrease in global settlement for column groups and 40% for individual columns, with greater effects at high loading levels. Beyond geometric parameters, cavity expansion during vibro-installation increases lateral earth pressure (K_0) by 20–50% and stiffness (up to 2 times the initial value) in a 1.5–2D zone. This yields 5– 25% global settlement reduction for column groups and 40% for individuals, with the latter dominant at high load levels [22,97,98].

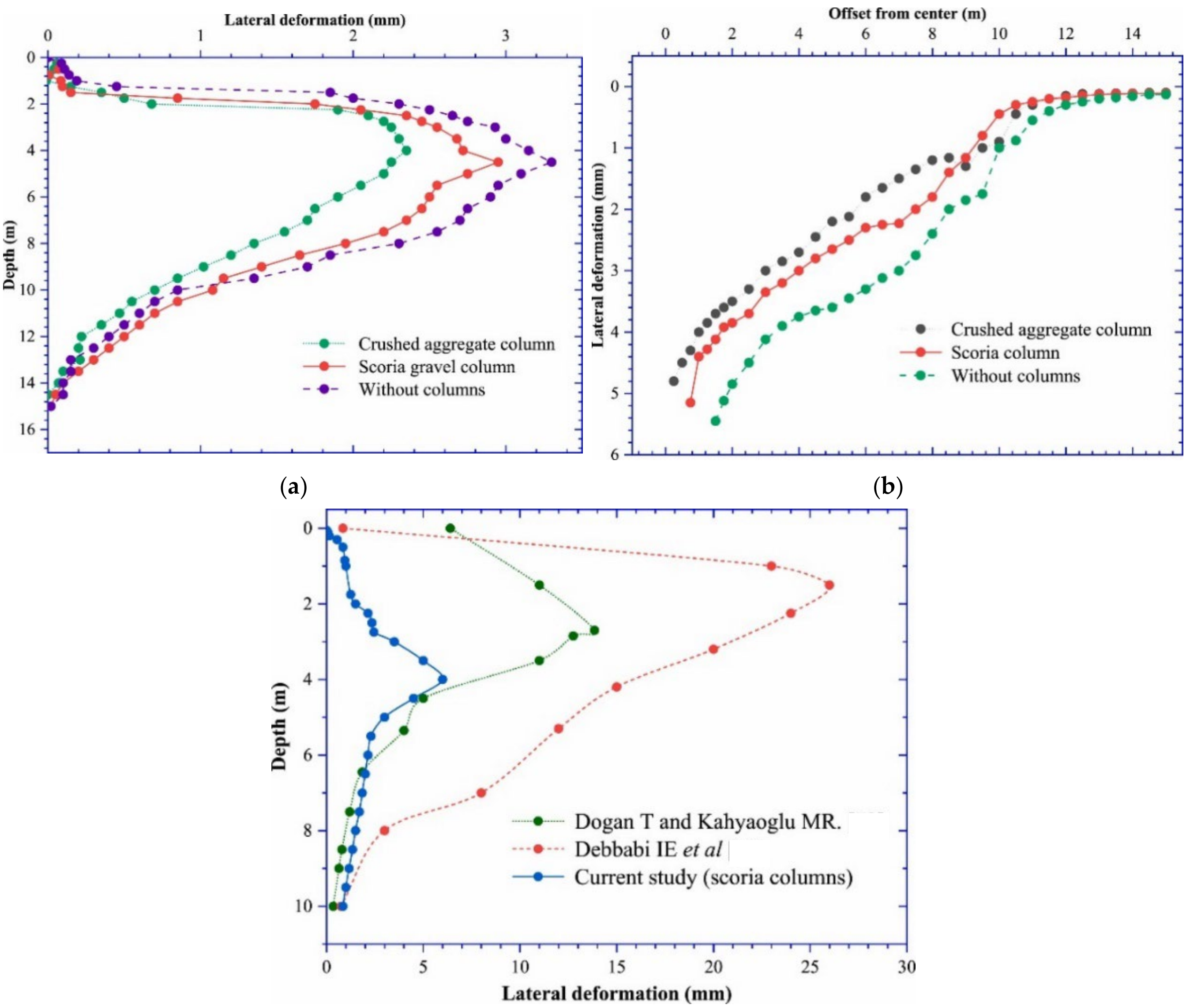

(**c**)

Figure 5. (**a**) Horizontal deformation and distance for SCs at a depth of 5 m below the ground level. (**b**) Horizontal deformation and depth curve for SCs at the center of the SC group. (**c**) Comparison of different types of stone [93].

3.4. Role of Geosynthetic Encasement

Geosynthetic encasement has transformed the performance of SCs in ultra-soft clays (c_u < 5 kPa) by overcoming the limitations of non-encased (or unencased) installations, as it provides hoop-tension confinement [5,48,91,99]. The encasement, usually geogrid or geotextile with tensile stiffness, J, ranging from 500 to 5000 kN/m, increases the lateral confining stress σ_h by 2 to 5 times, which reduces bulging and lateral stone loss [82,83,91,92]. This confinement mechanism leads to a 3–6 times greater improvement in ultimate bearing capacity, driven by higher interparticle friction and load transfer efficiency. The tensile strain is mobilized in the encasement under axial loading (ε_θ = 1–5%) before failure by hoop rupture. Mathematically, the optimal stiffness, J, of the encasement is proportional to the soil c_u, or stiffness, where lower strength soils require higher encasement stiffness for similar performance improvement. GESCs have been found to increase bearing capacity by a multiple of 3–4 times and to further increase the slope FS by 0–25% compared to OSCs [91,100,101].

Tan et al. [69] jointly utilized DEM and FDM modeling to improve understanding of geotextile-wrapped stone columns (GWSC) and their particle-scale interactions and geosynthetic confinement mechanisms under unidirectional compression loading. While the continuum-based FDM simulations provided the framework for modeling the GWSC entirely as a medium, the DEM-FDM model provided a more realistic representation of gravel shape, size distribution, and density and produced stress–strain curves matching experimental values. The multi-scale simulation also had success in reproducing local stress concentrations at the geotextile (Figure 6a), which were ultimately 2–3 times higher than the average membrane stress and were responsible for initiating puncture and progressive sleeve rupture. The continuum-based FDM model, however, hugely underestimated the ultimate bearing capacity, which was over 50%. This demonstrates the significant influence particle-geosynthetic interactions have on the confinement mechanism and failure of propagation in the wrapped columns (Figure 6b).

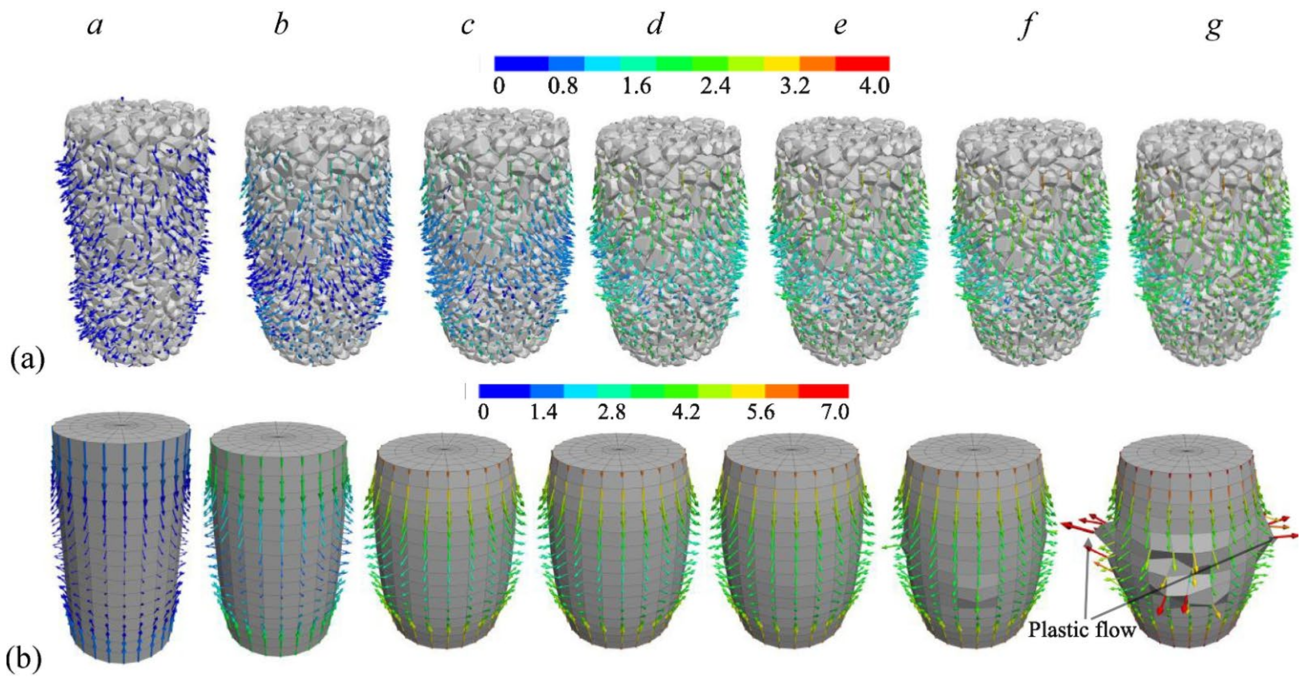

Figure 6. The displacement vectors of the SCs at different loading stages (unit: cm) (**a**) DEM model; (**b**) FLAC3D model [69].

However, a critical limitation of the study lies in its exclusion of soil–structure interaction. The surrounding soft soil was not simulated, and the resulting stress–strain response reflects the column behavior only. The soil response is not an in-place composite system performance, which means the design application is limited to the laboratory setting without suitable corrections for lateral boundary conditions [69,91,100]. Furthermore, the loading conditions were simplified to uniform top and bottom compression, thereby excluding all installation-induced anisotropy and field boundary stress redistribution effects. The research also indicated an effect of geotextile stiffness (Figures 7 and 8), as it was shown that stiffness slightly impacts ultimate strength but has a significant impact on initial modulus and deformation patterns of the column. The stiffness of higher geotextile stiffness restrained column deformation (displacements < 2 cm; (Figure 7a)), which led to improved confinement, while sleeves with lower stiffness permitted extreme bulging and "pie-shaped" deformations (Figure 7d). This finding reinforces the crucial role geosynthetic tensile stiffness has in controlling lateral expansion and elastic stiffness. However, geosynthetic stiffness has less effect on ultimate bearing capacity compared to tensile strength and interaction with the granular skeleton. Even though the analytical solutions based on numerical observations provided better predictions of mechanical response, the empirical correction factors used in the analysis indicate the present limitations in developing universal constitutive relationships for composite geosynthetic-encased aggregates.

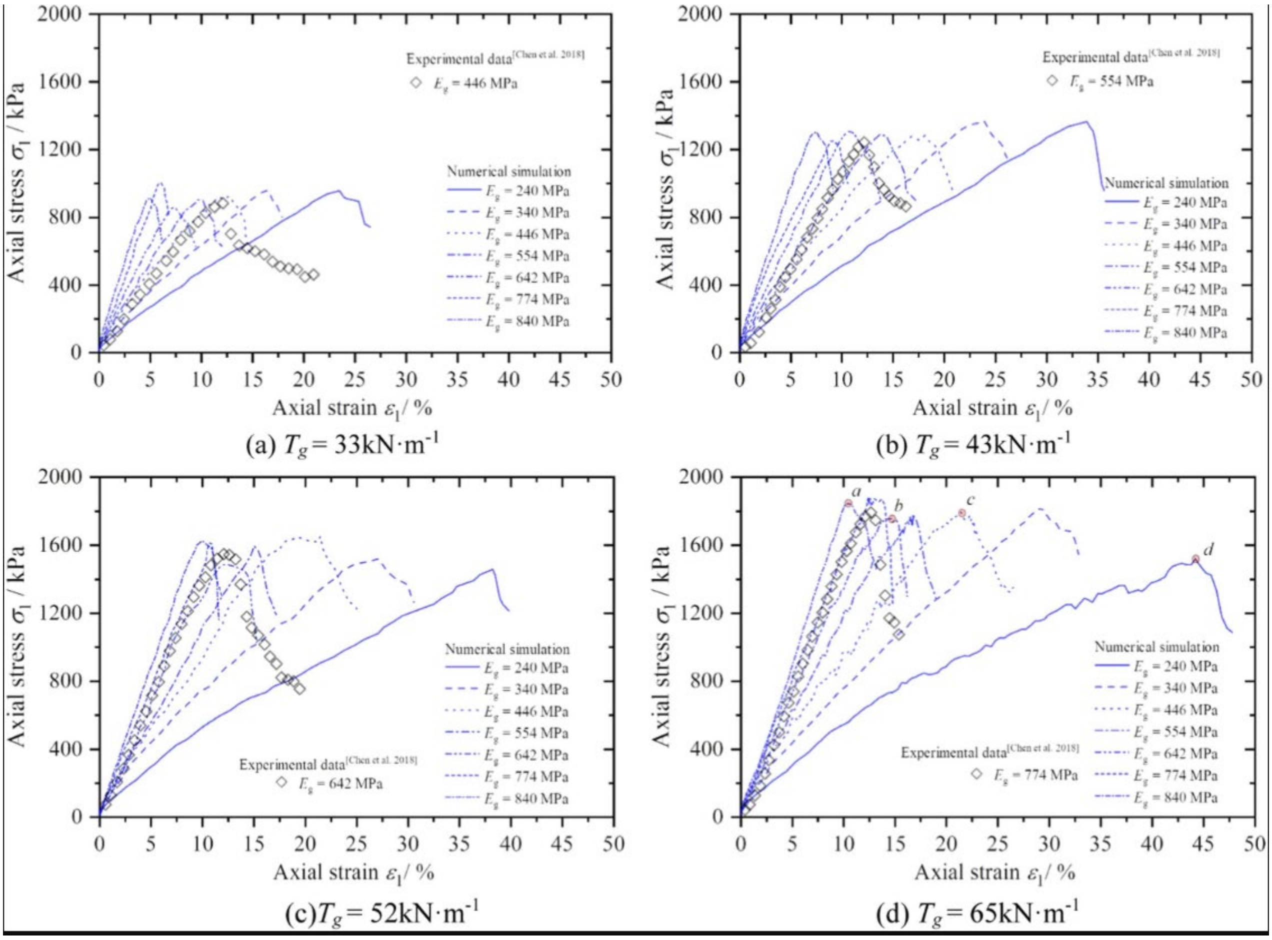

Figure 7. Stress–strain curves of wrapped stone columns with different geotextile stiffness [69].

Table 4 summarizes the quantitative effects of encasement stiffness, depth, geometry, and soil strength on the behavior of GESCs. The results consistently demonstrate that encasement stiffness (J > 2000 kN/m) and full-depth confinement (L > 10D) indicate the highest BCRs (5–7 times) and settlement reductions of up to 80%. Increasing J results in higher elastic stiffness of the column and lower lateral bulging (<5% radial strain), as evidenced by experimental studies [16] and similar findings in numerical modelling [94–98]. The diameter of the column has an inverse relationship to the improvement efficiency; smaller column diameters (0.6 m) achieved higher efficiency of stress concentration and hoop tension than the larger column diameter (1.0 m), which coincides with [102]. Performance improvements are most pronounced in ultra-soft soils (c_u < 5 kPa), where encasements contribute 5 times the improvements in lateral confinement (σ_h gain = 5 times) and 6 times improvements in bearing capacity. In terms of encasement type, geogrids perform better than woven geotextiles because they have higher tensile stiffness and interlocking ability, and hybrid geo-composite sleeves achieve the highest confinement efficiency (BCR = 5–7 times), albeit at slightly higher material cost. Overall, the results of this study emphasize that geosynthetic encasements change the load transfer mechanism by suppressing bulging, mobilizing hoop tension, and providing additional lateral confinement, all of which are important components to the stabilization of stone columns on very soft subgrades.

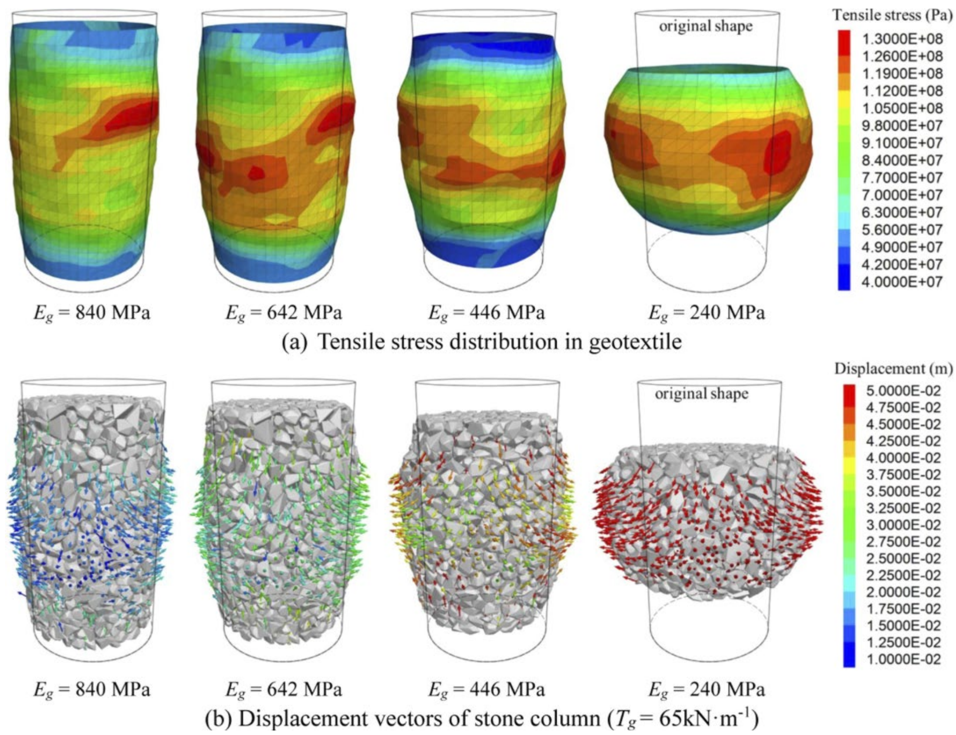

Figure 8. SC wrapped by geotextile with different stiffness at the peak strength state [69].

Table 4. Performance enhancement by encasement type/parameters.

Parameter	Range	BCR Gain	Settlement Reduction	Bulging Reduction ($\Delta r/r_o$)	Confining Stress Gain (σ_h)	Source
Encasement stiffness (J, kN/m)	500	2–3 times	50%	50% (<15%)	2 times	[16]
	2000–5000	4–6 times	70–80%	70% (<5%)	3–5 times	[60]
Encasement depth	Vertical (top 2D)	3 times	60%	60%	2.5 times	[20]
	Full (L > 10D)	5–7 times	80%	80%	4 times	[26,103]
Diameter (D)	0.6 m	5 times	75%	75%	+30% (vs. 1 m)	[89,96,100]
	1.0 m	3–4 times	60%	60%	Baseline	[102]
Soil cohesion (kPa)	<5	6 times	80%	80%	5 times	[61,62]
	20	3 times	50%	50%	2 times	[60,62,63]
Type	Geotextile	2–3 times	50%	50%	2 times	[17,69,71]
	Geogrid	4–6 times	70%	70%	4 times	[42,100,101]
	Hybrid	5–7 times	80%	80%	5 times	[10,48,103]

4. Construction Methods and Field Practices

This section provides insights into practical considerations for SC installation based on different advancements in vibro-replacement technique, quality control, and field applications on soft cohesive soils (c_u = 4–50 kPa). This includes the notion of selecting the best approach for installation (top-feed vs bottom-feed, wet vs dry), reducing construction flaws through automated monitoring, and coupling predictive models with an enhanced form of design.

4.1. Ordinary SC Installation

OSCs are typically constructed using vibro-replacement or vibro-displacement procedures, depending on the soil type and the stability of the borehole. The procedure uses an electric or hydraulic vibrating poker (vibroflot) operating at 30 to 50 Hz and with a range of motion of 5 to 25 mm. The vibroflot extends into the ground to the design depth, typically in the range of 5 to 20 m, creating a cylindrical cavity of 0.5 to 1.2 m in diameter through either a wet top-feed (i.e., water jetting) or dry bottom-feed (i.e., air flushing or mechanical extraction) method [11,51,97]. When the required depth is reached, granular backfill (typically crushed stone with a particle diameter of 20 to 75 mm) is introduced in sequential lifts of 0.3 to 1.0 m (Table 5). Each lift is then compacted radially using the subsequent vibration of the vibroflot to achieve a relative density in the range of 70 to 85%. In cohesive soils (c_u < 50 kPa), the wet top-feed method is normally employed because the water jetting helps with penetration and placement of the material, while the dry bottom-feed method is a better option for loose or unstable soils because it manages soils while maintaining borehole integrity [104,105].

Table 5. Comparison of vibro-replacement methods.

Method	Jetting Medium	Stone Supply	Soil Suitability (c_u, kPa)	Depth Range (m)	Advantages	Limitations	Field Examples	BCR Gain
Dry top-feed	Air flush	Surface hopper	>20 (kPa)—coarse or stiff soils	Shallow–medium (≤10)	Stable cavity; no water handling; clean operation	Unsuitable for very soft cohesive soils; risk of sidewall collapse	Lightly loaded industrial pads [105–107]	1.5–2.0
Wet top-feed	Water jet	Surface hopper	10–50 (kPa)—cohesive soils	Medium–deep (>10)	Effective removal of arisings; uniform column	Fine intrusion (5–10%); slurry softening; water disposal	Wastewater facility; embankment (failure at 7.9 m) [104,105]	2.0–3.0
Dry Bottom-Feed	Air flush	Poker-integrated hopper	4–20 (kPa)—very soft clays	Deep (≤20)	No fines intrusion (<2%); stable cavity; high control	Higher equipment cost	c_u = 10; c_u = 4–5); embankment (c_u = 15) [104,108,109]	2.5–4.0
Bottom-rammed	None	Driven tube	>30 (kPa)—stiff or granular soils	Shallow	High-density compaction; no jetting	Inefficient for soft soils; limited depth; costly	Franki pile variant [108,110,111]	=2.0

4.2. Encased Stone Column Construction

GESCs enhance traditional methods by incorporating geosynthetic sleeves for added confinement. The procedure starts similarly: a mandrel or vibroflot creates the borehole, but a geotextile/geogrid tube (tensile strength 20–100 kN/m) is pre-inserted or wrapped around the backfill [110–112]. The encasement is displaced using the vibroflot method, while in the replacement system, the encasement is placed after excavation. Backfill is placed in lifts and compacted for a density of 80 to 90%, and seams in the encasement can be sewn or can be overlapped, creating a uniform integrity. Recent studies include biodegradable encasements for sustainability and 3D-printed sleeves for custom stiffness [102–104,107]. Table 6 provides an overview of constructing GESCs using the dry bottom-feed vibro-replacement system, which promotes superior control and performance in very soft clays (c_u < 20 kPa) during construction [91,96,98,100]. The sequence: penetration, backfilling, compaction, finishing, typically takes between 17 and 28 min per 10 m column, with a small cost increase of approximately 15% in comparison to OSC. When combining very stiff encasement (J > 2000 kN/m), the dry method improves BCR by 5–7× due to very effective confinement, limited bulging, and stable cavity formation. Strict QA measures (depth log, current demand, and diameter uniformity) confer confidence that the columns remain intact and achieve reproducibility standards while working under soft ground conditions [16].

Table 6. Construction sequence for ESC procedures [91,96,98,100].

Step	Description	Duration (per Column, m)	Equipment	QA Check	Soft Soil Adaptation
1. Penetration	Vibroflot/mandrel with sleeve to design depth	4–8 min (10 m)	Vibroflot, crane	Depth log, current demand	Dry air flush; monitor pore water pressure < 50 kPa
2. Backfilling	Add gravel (4–40 mm) in lifts via the bottom hopper	8–12 min (10 m)	Hopper (0.3 m^3)	Volume: 0.28 m^3/m	Reduced lift (0.3 m) for c_u < 10
3. Compaction	Vibrate (40 Hz); tension sleeve	4–6 min (10 m)	Vibroflot	Diameter uniformity (±5%)	Stone consumption > 0.25 m^3/m
4. Finishing	Trim sleeve, integrity test	1–2 min	Manual	Seam overlap, no tears	Crust protection (no overworking)

4.3. Quality Control and Field Testing

Quality control (QC) ensures column integrity through monitoring and post-installation tests. During construction, parameters like vibration energy, backfill volume, and penetration rate are logged (e.g., via data acquisition systems). Post-installation, plate load tests (PLT) apply incremental loads (up to 1.5 times design) on a 1–3 m plate over the column, measuring settlement to verify capacity (acceptance: <25 mm at design load). Cone penetration tests (CPT) assess density via tip resistance. Other methods: dynamic cone penetration (DCP) for shallow checks and seismic tests for modulus. Recent AI-integrated monitoring systems use sensors to predict real-time QC with 95% accuracy. Challenges: variability in soft soils requires 10–20% testing coverage. Figure 9 presents the static load test setup, while Table 7 summarizes the key QC testing methods used to verify the performance and integrity of the stone and ESC after installation.

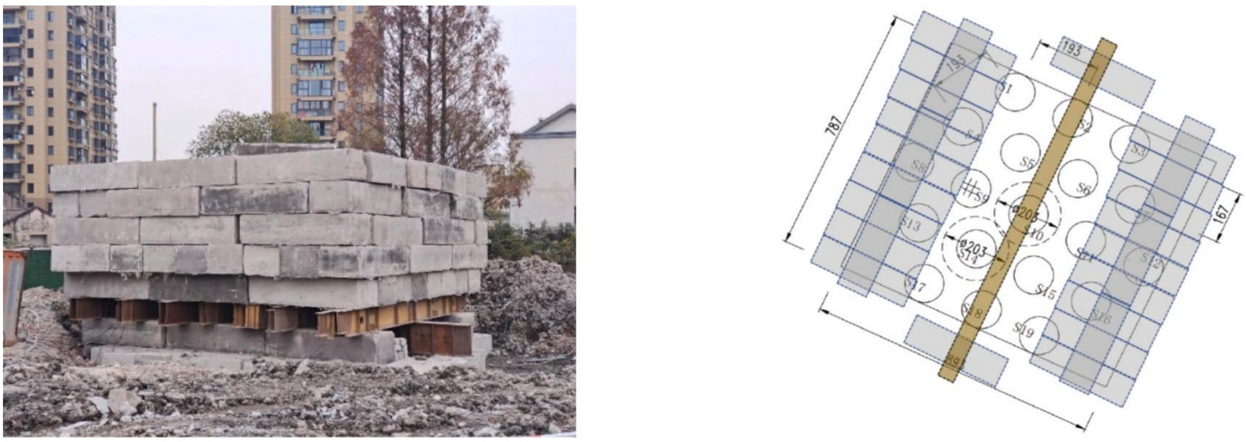

(a) (b)

Figure 9. Static load test: (**a**) test site, and (**b**) schematic diagram [12].

Table 7. Quality control testing methods.

Method	Purpose	Acceptance Criteria	Testing Frequency	Remarks/Reference
PLT	Verify ultimate bearing capacity and settlement performance	Settlement < 25 mm at design load (up to 1.5× design pressure)	1 per 50 columns	Measures load–settlement response; typical plate size 1–3 m; see Figure 9 [12].
CPT	Evaluate in situ density and column continuity	Tip resistance > 10 MPa	1 per 20 columns	Identifies weak zones and ensures uniform densification. [110–113]
DCP	Check the shallow integrity of the column head	>20 blows/m	Random verification	Quick surface QC; suitable for embankment and pad foundations. [114–116]
Seismic/Geophysical Tests	Assess stiffness and modulus variation	Vs > 200 m/s or consistent wave velocity	Selected columns	Non-destructive; complements CPT data. [108,114–116]

5. Experimental Investigations

Experimental studies are the foundation for understanding the behavior of SCs, and they are necessary to verify and validate the numerical models and ML predictions. Here, experimental studies conducted within the past three years were synthesized—both laboratory and large-scale testing—that provide insight into the load-carrying mechanisms, deformations, and performance improvements in soft soils. The controlled nature of the studies helps to highlight behaviors of the soil–column system, which can provide insight into things such as soil–column interaction, failure ratios, and optimization, and provides a channel to link the theoretical aspects to practical applications.

Laboratory model tests provide a controlled environment to investigate SC behavior and performance while enabling careful control of variables and minimizing variability associated with field studies [9,11,19,21,100]. Small-scale tests typically conducted at 1 g in large tanks (1–2 m) use scaled columns (D = 50–150 mm) with prepared soft clay beds (c_u = 5–30 kPa) to examine performance under static axial loading and cyclic loading [81]. The PLAXIS 3D investigations handled by McCabe et al. [81] indicated two main deformation modes for the 3 × 3 stone column group: punching and bulging, which are consistent with laboratory and numerical research conducted by Muir Wood et al. [117], McKelvey et al. [118], and Black et al. [119]. The short or closely spaced columns (L = 3 m, s (center-to-center spacing)) produced large vertical deformation beneath the base and a very small amount of horizontal deformation, indicating punching failure. The stress concentration ratio (σ'_c/σ'_{soil}) at depth decreased and approached unity due to side friction and load transfer diminishing.

On the other hand, in the longer length columns (L = 8–13.9 m), there was favorable evidence of large vertical and horizontal deformation occurring at approximately 2.5 m depth, marking the process of bulging failure. This is the principal failure mode for long columns installed at wider spacing. The stress ratio decreases locally at the bulging zone, but increases again with additional confinement. Overall, these results support the notion that column length and spacing are the relevant governing factors for the deformation mode rather than the overall group size. One limitation of the FEM approach is that, for simplicity of analysis, the soil was assumed to have uniform stiffness and may therefore not account for the crust's localized and shear effects, as well as the elastic degradation with depth.

Large-scale tests, conducted in pits or full-field setups (columns D = 0.6–1.0 m, depths 5–10 m), offer realism by incorporating installation effects and natural soil heterogeneity. These tests use heavy loading frames (capacities 100–500 kN) and monitor long-term consolidation via piezometers and inclinometers. The research conducted by Alkhorshid et al. [120] provides an innovative assessment of GESCs in very soft soil, examining woven geotextiles (G-1 to G-3) in-lab with varying stiffness and fills (sand, gravel, recycled construction, and demolition waste (RCDW)), as well as control tests. Additionally, three pressure cells (PC1, PC2, and PC3) were installed at different depths along the side of the column to measure lateral earth pressures. The results demonstrate that G-1 has a stiffness that increases the capacity of sand columns by twice at 50 mm of settlement compared to G-2, although G-2, using gravel, pushes ultimate loads 12 to 22.2% higher than sand while experiencing 9.5 to 15% more settlement due to particle breakage. The results also demonstrate that RCDW is consistently lower in 50 mm of ultimate loads when compared to sand and gravel throughout all of the geotextiles, although it should highlight the questionable sustainability of the aggregate, since poor performance was prevalent in only adding minute differences in aggregates (visuals may be lacking to fully assess suitability). Importantly, the maximum bulging occurred at 160 mm depth, affecting only PC1; PC2 and PC3 showed no response during loading. The G-2 column recorded greater lateral

https://doi.org/10.3390/jeta4020022

bulging than G-1, resulting in higher effective lateral pressures and a larger maximum earth pressure coefficient.

Additionally, the lateral pressures on the encasement reached passive Rankine levels. While Priebe [121] and Gäb et al. [122] recommend K = 1 for design, and Baumann and Bauer [123] suggest K between at-rest and passive, this study confirms pressures attain a full passive state under load. The findings contribute toward understanding embankment design performance and considerations on sustainability; however, consideration related to RCDW long-term degradation, as well as cost–benefit analysis within considerations for very soft soils, was not overlooked.

6. Machine Learning and Data-Driven Models

6.1. Introduction to Data-Driven Modeling

ML and data-driven modeling have introduced significant advancements in geotechnical engineering and offer predictive tools that can complement traditional experimental and numerical approaches. In this section, a review of recent advances in the application of ML to predict the performance of stone columns, including types of models, datasets, evaluation metrics, and comparisons with numerical methods, is presented. ML methods capture the complexities of the soil–column interactions and lead to reasonably rapid and precise predictions of bearing capacity and settlement, which are necessary to improve designs in soft soil conditions [36,37,39,41,124,125]. The concept of data-driven modeling, which is an ML-based modeling approach, captures patterns that arise in complex datasets without investing in physical modeling or expensive experiments. In terms of geotechnical engineering, soil properties and structures respond nonlinearly, making ML models an ideal tool to capture multivariate relationships. Therefore, methods based on ML modeling are adaptable to varying conditions and predict bearing capacity and settlement outcomes with accuracies above 95%. In recent literature, some studies describe the use of ML integrated with real-time monitoring of the field conditions to reduce design costs in geotechnical engineering by 20–30% along the project, allowing for predictive maintenance [36,37]. ML-based modeling applications include estimating the performance of stone columns and optimizing encasement parameters, as well as estimating long-term behaviors. While current datasets and model interpretability pose challenges, recent advances in openly accessible repositories and physics-informed ML are overcoming these issues through sustainable design practices globally.

6.2. Overview of ML Models Used for SCs Prediction

Despite significant strides in the field, traditional methods—experimental testing, regression analysis, analytical formulations, and numerical simulations—often struggle to accurately predict the ultimate bearing capacity due to the complex, nonlinear interactions between governing parameters. Advances in computing technologies provide support to intelligent computing approaches, such as ANN, to numerically model these complex relationships in engineering applications [36,37]. For example, Kuo and Jaksa [126] used artificial neural networks to assess the bearing capacities of strip footings and SCs in layered cohesive soils. Momeni et al. [127] produced ANN models that incorporated genetic algorithms to reliably predict the capacity of piles, showing that genetic algorithms improved the capacity prediction accuracy for both piles and stone columns. Chik et al. [128] used multilayer perceptron (MLP) ANNs to forecast the settlement of embankments supported by SCs, demonstrating that the MLP ANN would yield accurate predictions of the settlements. Aljanabi and Chik [44] utilized SVM inventively to predict stone column capacities and validated their statistical results that predicted remarkably low errors, as presented in Table 8.

Mosallanezhad and Moayedi [129] proposed a hybrid ANN method to estimate uplift resistance of screw piles, emphasizing its efficiency in predicting resistance capacities. Sahu and Patra [130] utilized ANNs to estimate the capacities of strip foundations built on geosynthetic soil reinforcement and produced an empirical equation with excellent predictive power. Moayedi and Rezaei [131] established a practical ANN-based correlation for bearing capacity of SCs, with a mean absolute error (MAE) of less than 0.262. Das and Dey [132] compared three Adaptive Neuro-Fuzzy Inference System (ANFIS) types: ANFIS-E (experimental data only), ANFIS-A (analytical/numerical data), and ANFIS-EA (combined data); of the three methods, the hybrid ANFIS-EA model performed best. In addition, Das and Dey [43] compared SVR and ANN models for predicting ultimate SC capacities, with SVR performing better in predictive accuracy. Dey and Debnath [133] compared SVR variations (ERBF, POLY, and RBF) on geogrid reinforced sand beds and found that SVR-ERBF predicted results most accurately with minimal errors. Lastly, Mazumder and Garg [134] applied linear regression, SVM, Gaussian Process Regression (GPR), and ANN in MATLAB R2021a User Interface (2021) to model radial strain and capacity of SCs and found ANN to yield the highest accuracy.

Employing feed-forward (FFNN) and time-delay (FTDNN) neural networks based on CPT data, Moayedi and Hayati [135] assessed axial load-settlement behavior of piles and drilling columns to validate their suitability for single-pile design. Jahed Armaghani and Shoib [136] applied neural networks with Particle Swarm Optimization (PSO) to predict socketed pile bearing loads. Bagińska and Srokosz [137] implemented Deep Neural Networks (DNNs) for shallow column ultimate capacity prediction and proved their effectiveness over large datasets. Finally, Sethy and Patra [138] used neural networks to estimate the capacities of circular foundations on sand layers, demonstrating that this type of analysis supports the design process in practice. Ardakani and Dinarvand [139] optimized the prediction of GESCs using ANNs calibrated by a Colonial Competitive Algorithm (ANN-ICA), which was superior to conventional ANNs. Ghanizadeh and Ghanizadeh [140] employed Multivariate Adaptive Regression Splines (MARS) and Escaping Bird Search Optimization (EBS) to create a GESC model and found that increases in an input parameter increased capacity. Gnananandarao and Onyelowe [141] applied ANNs to predict the performance of reinforced SCs on soft soils. Lafifi and Rouaiguia [141] combined response surface methodology and ANNs with multi-objective genetic algorithms (MOGA) aimed at optimizing geosynthetic-reinforced sandy foundation parameters. Finally, Zeini and Lwti [125] predicted the capacity of a geogrid-reinforced sand bed using multivariate polynomial regression (MPR), RF, and linear regression (LR), and found that RF had the best performance based on the statistical evaluations.

Among the various ML approaches applied to predict the bearing capacity and settlement of SCs, hybrid metaheuristic–ML models (such as Artificial Bee Colony optimized Artificial Neural Networks (ABC-ANN) and harmony search optimized SVR (HS-SVR)) demonstrated the highest predictive accuracy, achieving R^2 values between 0.981 and 0.989 with minimal error rates. Similarly, SVR with an exponential radial basis function kernel (SVR-ERBF) and extreme gradient boosting (XGBoost) consistently outperformed conventional models in terms of accuracy and generalization capability. These models excel due to their robust handling of nonlinear parameter interactions, effective regularization mechanisms that mitigate overfitting on relatively small geotechnical datasets, and, in the case of ensemble and white-box variants, enhanced interpretability. A detailed comparison of the reviewed ML models, including performance metrics (R^2 and RMSE), dataset characteristics, and key limitations, is presented in Table 8.

https://doi.org/10.3390/jeta4020022

Table 8. Summary of ML models applied to stone column prediction.

Ref.	Model Type	Hybrid/Optimization	Input Parameters	Output	Dataset Size/Source	Key Results
[124]	LR	No	-	Bearing capacity	Combined experimental and field test data	R^2 = 0.848, RMSE = 1922.12, MAE = 14,449.63
	SVR	No	-			R^2 = 0.169, RMSE = 53,378.71, MAE = 20,497.13
	GB	Ensemble	-			R^2 = 0.986, RMSE = 5806.08, MAE = 1697.49
	KNN	Ensemble	-			R^2 = 0.987, RMSE = 5593.26, MAE = 1668.71
[40]	ABC	ABC optimization	GLD/FD ratio, Lsc/dsc ratio, SCS/D footing ratio	Bearing capacity	-	R^2 = 0.981–0.989, error rates = 7.86×10^{-5} to 0.00883
	HS	HS optimization				R^2 = 0.984–0.988, error rates = 3×10^{-5} to 0.00551
[125]	MPR	No-(White-box ML model)	Geogrid-reinforced sandy bed and geogrid-ECS (e.g., footing and soil properties, reinforcement characteristics)	Bearing capacity	245 experimental results	MPR (Train/Test R^2 = 0.994/0.983; RMSE = 13.01/15.66) SVR-ERBF (0.999/0.989; 4.30/11.45) SVR-RBF (0.980/0.975; 17.63/17.51) SVR-POLY (0.976/0.965; 20.63/23.93) ANFIS (0.996/0.981; 7.90/13.80)
[44]	SVR—e-RBF and ν-RBF models	No	column geometry, soil properties, loading conditions)	Settlement behavior (prediction of the settlement of SCs)	Field-monitored data used for model training and validation	e-RBF model: RMSE = 0.002686–0.003281; MAE = 0.040–0.045; ν-RBF model: RMSE = 0.002398–0.003278; MAE = 0.037–0.045; ν-SVM with RBF kernel and 10-fold cross-validation achieved the best accuracy (R = 0.9987).
[142]	LR, SVR, GPR, and ANN	No	Various geometric and material parameters of sustainable recycled materials within SCs	Bearing capacity	45 constructed samples used for model development and validation	LR: (R^2 = 0.956, RMSE = 7.662 kPa, MAE = 5.846 kPa). ANN: (R^2 = 0.974, RMSE = 5.897 kPa, MAE = 4.817 kPa). ANN model exhibited superior predictive accuracy compared to MLR, SVM, and GPR.

Where GB—Gradient Boosting; KNN—K-Nearest Neighbors; GLD/FD ratio—Ratios of geogrid-reinforced layer diameter to footing diameter; Lsc/dsc ratio—SCs length to diameter, SCS/Dfooting ratio—Settlement to footing diameter; MPR—Multivariate Polynomial Regression; GPR—Gaussian Process Regression.

6.3. Comparison with Traditional Numerical Models

While advancements have been made in the area of research, conventional methods composed of experimental testing, regression analysis, analytical formulations, or numerical simulations (FEM/DEM) can have difficulty reliably predicting the ultimate bearing capacity due to complex, nonlinear interactions among governing parameters. To clearly illustrate the strengths, limitations, consistency, and inconsistency among the different methodologies, a comparative summary is presented in Table 9. As presented in Table 9, ML models excel in handling nonlinear relationships and optimization tasks, while numerical methods remain superior for detailed mechanistic understanding.

Table 9. Comparison of analytical, numerical, and ML approaches for SCs analysis.

Aspect	Analytical or Empirical Methods	Numerical Modeling (FEM/DEM)	ML Approaches
Accuracy	Moderate	High	Very High (R^2 often > 0.95)
Computational cost	Very Low	High (especially 3D)	Low (after training)
Physical interpretability	High	Very High	Moderate to Low (Black-box nature)
Handling complex interactions	Limited	Excellent	Excellent
Data requirement	Low	Moderate	High
Time for prediction	Very fast	Slow	Very fast
Main advantages	Simple, easy to apply	Captures detailed mechanisms	Rapid prediction & optimization
Main limitations	Oversimplifies real behavior	Computationally expensive	Needs quality data, limited generalization
Best used for	Preliminary design	Detailed mechanism studies	Fast prediction & design optimization

ML models perform better than traditional numerical methods in terms of efficiency and flexibility. For several ML models to efficaciously operate, the user's input is significantly less than that required for the FEM approach; for example, the FEM approach requires detailed constitutive models (i.e., Mohr–Coulomb parameters) and substantial computing power (10–50 h for 3D) resulting in 10–20% errors due to parameter uncertainty, whereas ML can be trained within minutes to achieve $R^2 > 0.98$ even with minimal training data. For example, an XGBoost model predicted ultimate bearing capacity 25% faster than FLAC3D while yielding 8% less RMSE [26,143]. It is also important to mention the advantages of using the FEM method in being able to model the subject physical mechanisms (i.e., bulging stress fields), while ML, as a method, is dependent upon the quality of the dataset to reach its performance outcome (i.e., general ability to make predictions). Importantly, ML models are not purely black-box approaches disconnected from mechanics. Feature importance analyses in several studies consistently reveal that c_u, spacing-to-diameter ratio (s/D), and encasement stiffness (J) are the most influential parameters. These variables directly correspond to the fundamental physical mechanisms of bulging, lateral confinement, and load transfer through soil arching. This strong alignment demonstrates that well-trained ML models effectively capture the underlying geotechnical behavior rather than merely fitting data statistically.

Hybrid ML-FEM methods integrate physics-informed constraints into ML models, resulting in performance outcomes where error is <3% that embed Mohr–Coulomb parameters [138,143–145]. To further strengthen this linkage between mechanics and data-driven modeling, the most promising direction is the adoption of physics-informed neural networks (PINNs), which embed governing equations (such as arching theory and consolidation models) directly into the loss function. This approach improves both predictive accuracy and physical consistency of the models. Limitations include ML as a "black box" method and the degree of dependence on datasets in predictive ability, requiring a physics-guided integration framework to increase reliability.

While several ML techniques have demonstrated strong potential, not all are universally applicable. Simple linear regression and non-optimized basic artificial neural networks frequently exhibit poor performance and high overfitting when applied to the small and often noisy datasets typical in stone column research. Models developed solely on numerical (FEM/DEM) data without adequate experimental or field validation are also unreliable for practical use, as they tend to ignore critical scale effects and installation disturbances. Additionally, opaque black-box models (such as standard ANNs without interpretability tools) should be avoided in high-stakes projects unless combined with uncertainty quantification methods, because they provide limited physical understanding and may hinder engineering judgment.

7. Challenges and Research Gaps

There has been notable progress in various SC technologies (e.g., unencased and encased), but some challenges and research gaps remain, hindering experimental, numerical, and ML methods from achieving their potential. This section provides a critical overview of key challenges, highlighting recent studies, and identifies aspects that require more investigation to advance the design, prediction, and sustainability of stone columns in applications on soft soils. Many ML models (e.g., ANN, SVR, and XGBoost, mostly) developed for SCs are highly reliant on robust datasets to reach high prediction accuracy ($R^2 > 0.95$) for responses such as bearing capacity or settlement. However, geotechnical datasets in the SCs literature remain limited, typically ranging between 37 to 901 samples in studies. These datasets arise from experimental tests or numerical simulations and generally do not reflect a diverse range of soil types (e.g., c_u = 5–50 kPa), column configurations (D = 0.5–1.2 m, s/D = 2–4), and loading conditions (static or cyclic). Lack of open-access, standardized repositories limits model generalization and increases the probability of models 'overfitting' the data (e.g., they drop 10–15% from prediction accuracy on new data). Some recent works have suggested platforms that offer open-access data, but currently, the papers of only 20% have data publicly available to share to assist further ML work with SCs [12,110,144–147]. Global initiatives are necessary for further standards of open-access, large datasets, and could even potentially include IoT-type field monitoring to help expand datasets of this type.

GESCs provide enhanced performance using geosynthetic encasement; however, the absence of standardized design parameters, the encasement stiffness (J = 500–3000 kN/m), the length (whether partial or full), and encasement material type (geotextile or geogrid)—complicates the design process. J > 1500 kN/m has been revealed to optimize confinement of the stone columns in soft clays (c_u < 15 kPa), but variations in seam strength and method of installation lead to inconsistent BCR. Furthermore, field test results demonstrate a 20–30% variability in GESC performance due to a lack of standardization. Challenges in standardization limit the ability to scale up the design and be cost-effective when deployed in geotechnical construction practice. Existing design codes provide little guidance on hybrid encasements that use both types of encasement materials. Informed standardization through parametric studies and ML-based optimization could reduce the variability of design parameters by 15 to 25%, facilitating increased performance in various geotechnical applications.

Time-dependent behavior, such as creep and consolidation, influences the longevity of SCs. However, the effect of creep and consolidation is under-investigated. Creep, or strain rate, has been recognized as a source of long-term settlements in soft soils totaling up to a 10 to 20% increase over a period of 5 to 10 years. Consolidation is primarily concerned with the drainage rate. Since 2023, only 10% of the published studies have considered these factors, and the FEM studies using soft soil creep to predict about 50–70% of settlement are limited by not including time scales of more than 10 years. In addition to the limited studies on phenomena associated with creep, which were limited to centrifuge tests watching short-term cyclic aspects, there is a lack of experimental data on creep. Furthermore, ML modelling does not consider time-dependent features on a large scale, leading to decreased confidence in long-term predictions of performance. Identifying these creeps to better predict long-term factors requires field studies over long-time periods and incorporating time-dependent viscoelastic models within hybrid ML models, which can help reduce predictability error by 20% with timeliness of prediction considered.

While ML models can achieve very high accuracy (R^2 = 0.98–0.999), a major limitation is their black-box nature, which restricts interpretability and can undermine trust when applied to safety-critical geotechnical designs. In engineering practice, designers and regulatory authorities require transparent justification of predictions. To address this, the integration of Explainable AI (XAI) techniques—such as SHAP (SHapley Additive exPlanations), LIME, and feature importance analysis—offers a promising solution. These methods can quantify the contribution of key input parameters and provide physically meaningful insights, thereby enhancing model transparency and promoting greater acceptance of ML tools in practice. Complementing XAI, hybrid physics-informed ML (PI-ML) models integrate governing physical equations (e.g., Mohr–Coulomb failure criterion and consolidation theory) directly into the learning process. This approach combines the predictive power of data-driven models with physical consistency, achieving high accuracy (R^2 = 0.99) using up to 30% less data than conventional ANN models. However, physics-informed modeling is still emerging and faces challenges, including the complex integration of FEM outputs (e.g., stress fields) into the loss function and increased computational cost (typically 2–5 times longer training time compared to standard ML). Developing scalable, open-source frameworks for physics-informed and XAI-enhanced hybrid models could reduce prediction errors by 5–10% and significantly improve confidence in real-time design optimization.

8. Limitations and Future Research Directions

Despite the comprehensive nature of this review, several limitations should be acknowledged. Most studies rely on limited open-access datasets, and many ML models suffer from the black-box nature, reducing interpretability. Laboratory tests often overlook scale effects, while long-term field data on creep and consolidation remain scarce. Additionally, a noticeable regional bias exists, with the majority of research concentrated in specific geographical areas.

To overcome these limitations, focused future research is essential. Key areas include: (1) creation of global open-access repositories with more than 1000 samples (c_u = 5–50 kPa, s/D = 2–4) from experimental, field, and FEM/DEM studies to improve predictive accuracy by 10–15% and reduce overfitting; (2) development of coupled ML-numerical digital twin systems combining XGBoost with PLAXIS 3D (R^2 = 0.99) to embed Mohr–Coulomb constraints, significantly reducing data needs and simulation time; (3) conducting sustainability Life Cycle Assessments (LCAs) per ISO 14040 [148] to evaluate vibroflot energy consumption and waste impacts, aiming for 15% design savings and 20–30% CO_2 reduction through ML-optimized designs; and (4) implementation of IoT-ANN real-time monitoring systems (95% accuracy) for dynamic optimization during construction and long-term prediction of creep and consolidation up to 10–20 years.

9. Conclusions

(a) This review presents a synthesis of experimental, numerical (FEM/DEM), and machine learning methods for investigating stone columns, and more importantly, demonstrates hybrid machine learning models (R^2 = 0.981–0.989) that represent superior predictive accuracy and computational efficiency in exchange for traditional, single-domain methods and directly addresses existing gaps in past literature, which has investigated stone columns in isolation with either experimental or numerical methods. It discusses that up to 60–80% of the load is transferred via an arching mechanism with pre-determined laboratory, field, and 3D FEM studies demonstrating stress concentration ratios, while enhancing composite stiffness has reduced settlements by 50–80% soft clay foundations.

(b) Supplies an extensive assessment of bulging failure (c_u = 15–25 kPa, bearing capacity = $4c_u$ $(D/L)^{0.5}$), punching failure (c_u < 10 kPa, settlement > 10%D), and shear failure (s > 3D, BCR < 2.0) with hybrid modes happening in 60% of published cases and confirmed through Mohr–Coulomb FEM simulations. Provides optimal spacing s/D = 2–3, generating BCR improvements of 50–100% and diameter D = 0.8–1.2 m, improving capacity by 30 to 50%, all enhanced by the impact of vibro installation. Based on analysis of 245 experimental datasets, geosynthetic encasement (J > 2000 kN/m) produced a 3 to 6 times increase in BCR of c_u < 15 kPa with bulging reduction of 70–80%, and settlement reductions of 50–80%, with geogrids yielding 2 times more confinement improvement than geotextiles.

(c) A dry bottom-feeding installation for very soft clays (c_u = 4–20 kPa), which can achieve a BCR = 2.5–4.0 with less than 2% fines intrusion and a relative density of approximately 80 to 90% for 10 m columns installed in 17–28 min, using an embankment validation study.

(d) Machine learning has been proven superior, achieving 25% faster computation times than FLAC3D train ML and near-equal accuracy (<5% error). XGBoost (R^2 = 0.9947, RMSE = 4.8 kPa) and hybrid methods (HS–SVR$-R^2$ = 0.984–0.988) enable rapid optimization of designs (37–901 samples) using sparsely available datasets.

(e) Critical gaps in knowledge exist in datasets, time-dependent behaviors (creep/consolidation; 10–20% long-term settlement over five to ten years), and information integration with physics and ML to better generalize models and ensure long-term reliability.

(f) Suggests disruptive innovations such as open-access repositories, physics-informed neural networks, digital twins (R^2 = 0.99 R^2, time reduced by 50%), AI real-time monitoring (95% accuracy on settlements), resulting in a 15–30% reduction in design costs per ISO 14040 LCA standards.

Finally, it aligns with trends in global AI-geotechnics, optimally applied to zipper embankment and foundation applications in computers and geotechnics, advancing sustainable solutions to the challenges posed by increasingly soft soil in worldwide infrastructure projects.

Author Contributions: Conceptualization, M.A. and A.E. (Ayman ELtahrany); Methodology, M.A.; Software, M.A.; Validation, M.A., A.E. (Ayman ELtahrany) and A.E. (Amr ElNemr); Formal Analysis, M.A.; Investigation, M.A.; Resources, M.A. and A.E. (Ayman ELtahrany); Data Curation, M.A.; Writing—Original Draft Preparation, M.A.; Writing—Review & Editing, M.A., A.E. (Ayman ELtahrany) and A.E. (Amr ElNemr); Visualization, M.A.; Supervision, A.E. (Ayman ELtahrany) and A.E. (Amr ElNemr); Project Administration, M.A.; Funding Acquisition, M.A. All authors have read and agreed to the published version of the manuscript.

Funding: The authors did not receive support from any organization for the submitted work.

Institutional Review Board Statement: Not applicable.

Data Availability Statement: No new data were created or analyzed in this study.

Conflicts of Interest: The authors declare no conflict of interest.

References

1. Onyelowe, K.C.; Ebid, A.M.; Sujatha, E.R.; Fazel-Mojtahedi, F.; Golaghaei-Darzi, A.; Kontoni, D.P.N.; Nooralddin-Othman, N. Extensive overview of soil constitutive relations and applications for geotechnical engineering problems. *Heliyon* **2023**, *9*, e14465. [CrossRef]
2. Azam, F.A.A.; Omar, R.C.; Roslan, R.; Baharudin, I.N.Z.; Razman, M.Z.A. Mechanical behavior, compressibility, and microstructural analysis of problematic soil through a green soil stabilization approach. *Results Eng.* **2024**, *24*, 103524. [CrossRef]
3. Bao, X.; Li, J.; Shen, J.; Chen, X.; Zhang, C.; Cui, H. Comprehensive multivariate joint distribution model for marine soft soil based on the vine copula. *Comput. Geotech.* **2025**, *177*, 106814. [CrossRef]
4. Ngo, D.H.; Horpibulsuk, S.; Suddeepong, A.; Hoy, M.; Chinkulkijniwat, A.; Arulrajah, A.; Chaiwan, A. Compressibility of ultra-soft soil in the Mae Moh Mine, Thailand. *Eng. Geol.* **2020**, *271*, 105594. [CrossRef]
5. Yang, Q.; Zheng, Z.; El Naggar, M.H.; Kong, G.; Zhang, S.; Yang, G.; Ren, Y. Experimental study of the interface evolution behavior and softening mechanism of structure-marine soil. *Soils Found.* **2023**, *63*, 101324. [CrossRef]
6. Fu, H.; Wang, J.; Cai, Y.; Jin, J.; Dong, Q.; Hu, X.; Wang, P.; Geng, X.; Zhang, D. Field study of monotonic and cyclic lateral behaviour of piles in soft soils improved with and without vacuum preloading. *Acta Geotech.* **2020**, *15*, 3183–3192. [CrossRef]
7. Chu, J.; Bo, M.W.; Choa, V. Practical considerations for using vertical drains in soil improvement projects. *Geotext. Geomembr.* **2004**, *22*, 101–117. [CrossRef]
8. Nakao, K.; Inazumi, S.; Takaue, T.; Tanaka, S.; Shinoi, T. Visual evaluation of relative deep mixing method type of ground-improvement method. *Results Eng.* **2021**, *10*, 100233. [CrossRef]
9. Yi, Y.; Liu, S.; Puppala, A.J.; Jing, F. Variable-diameter deep mixing column for multi-layered soft ground improvement: Laboratory modeling and field application. *Soils Found.* **2019**, *59*, 633–643. [CrossRef]
10. Inazumi, S.; Shakya, S. A Comprehensive Review of Sustainable Assessment and Innovation in Jet Grouting Technologies. *Sustainability* **2024**, *16*, 4113. [CrossRef]
11. Verma, P.; Wijewickreme, D. Laboratory assessment of the effect of vibro-replacement ground improvement on the mechanical response of natural silt. *Soil Dyn. Earthq. Eng.* **2023**, *173*, 108059. [CrossRef]

12. Xia, C.; Shi, X.; Hu, A.; Chen, Y.; Jalal, F.E.; Chen, X. Consolidation analysis of composite ground with stone column using a composite column-soil element model coupled seepage characteristics. *Comput. Geotech.* **2025**, *180*, 107064. [CrossRef]
13. Christoulas, S.; Bouckovalas, G.; Giannaros, C. An Experimental Study on Model Stone Columns. *Soils Found.* **2000**, *40*, 11–22. [CrossRef] [PubMed]
14. Dash, S.K.; Bora, M.C. Improved performance of soft clay foundations using stone columns and geocell-sand mattress. *Geotext. Geomembr.* **2013**, *41*, 26–35. [CrossRef]
15. Yoo, C.; Abbas, Q. Performance of geosynthetic-encased stone column-improved soft clay under vertical cyclic loading. *Soils Found.* **2019**, *59*, 1875–1890. [CrossRef]
16. Ayadat, T.; Hanna, A.M. Encapsulated stone columns as a soil improvement technique for collapsible soil. *Ground Improv.* **2005**, *9*, 137–147. [CrossRef]
17. Almeida, M.S.S.; Hosseinpour, I.; Riccio, M.; Alexiew, D. Behavior of Geotextile-Encased Granular Columns Supporting Test Embankment on Soft Deposit. *J. Geotech. Geoenviron. Eng.* **2015**, *141*, 04014116. [CrossRef]
18. Pandey, B.K.; Rajesh, S.; Chandra, S. Performance enhancement of encased stone column with conductive natural geotextile under k0 stress condition. *Geotext. Geomembr.* **2021**, *49*, 1095–1106. [CrossRef]
19. Xu, F.; Moayedi, H.; Foong, L.K.; Moghadam, M.J.; Zangeneh, M. Laboratory and numerical analysis of geogrid encased stone columns. *Measurement* **2021**, *169*, 108369. [CrossRef]
20. Malarvizhi, S.N. Comparative study on the behavior of encased stone column and conventional stone column. *Soils Found.* **2007**, *47*, 873–885. [CrossRef]
21. Pandey, B.K.; Rajesh, S.; Chandra, S. Time-Dependent Behavior of Embankment Resting on Soft clay Reinforced with Encased Stone Columns. *Transp. Geotech.* **2022**, *36*, 100809. [CrossRef]
22. Yoo, C. Settlement behavior of embankment on geosynthetic-encased stone column installed soft ground—A numerical investigation. *Geotext. Geomembr.* **2015**, *43*, 484–492. [CrossRef]
23. Chen, J.F.; Li, L.Y.; Xue, J.F.; Feng, S.Z. Failure mechanism of geosynthetic-encased stone columns in soft soils under embankment. *Geotext. Geomembr.* **2015**, *43*, 424–431. [CrossRef]
24. Schnaid, F.; Winter, D.; Silva, A.E.F.; Alexiew, D.; Küster, V. Geotextile encased columns (GEC) used as pressure-relief system. Instrumented bridge abutment case study on soft soil. *Geotext. Geomembr.* **2017**, *45*, 227–236. [CrossRef]
25. Abdelhamid, M.; Ali, N.; Abdelaziz, T. A Literature Review of Factors Affecting the Behavior of Encased Stone Columns. *Geotech. Geol. Eng.* **2023**, *41*, 3253–3288. [CrossRef]
26. Abdelbaset, A.; Arafa, I.T. Improvement of consolidation settlement beneath square footings using uncased and encased stone columns. *Structures* **2023**, *58*, 105609. [CrossRef]
27. Tang, L.; Cong, S.; Ling, X.; Lu, J.; Elgamal, A. Numerical study on ground improvement for liquefaction mitigation using stone columns encased with geosynthetics. *Geotext. Geomembr.* **2015**, *43*, 190–195. [CrossRef]
28. Ashour, S.; Ghataora, G.; Jefferson, I. Behaviour of Model Stone Column Subjected to Cyclic Loading. *Transp. Geotech.* **2022**, *35*, 100777. [CrossRef]
29. Ghazavi, M.; Yamchi, A.E.; Afshar, J.N. Bearing capacity of horizontally layered geosynthetic reinforced stone columns. *Geotext. Geomembr.* **2018**, *46*, 312–318. [CrossRef]
30. Kelesoglu, M.K.; Durmus, C. Numerical Plane-Strain Modelling of Stone Columns: Installation Process, Single and Group Column Behaviour. *KSCE J. Civ. Eng.* **2022**, *26*, 3402–3415. [CrossRef]
31. Abdelhamid, M.; Ali, N.; Abdelaziz, T. Experimental Study on the Behavior of Floating Encased Stone Columns in Collapsible Soils. *Indian Geotech. J.* **2026**, *56*, 1423–1444. [CrossRef]
32. Tai, P.; Indraratna, B.; Rujikiatkamjorn, C. Experimental simulation and mathematical modelling of clogging in stone column. *Can. Geotech. J.* **2018**, *55*, 427–436. [CrossRef]
33. Nav, M.A.; Rahnavard, R.; Noorzad, A.; Napolitano, R. Numerical evaluation of the behavior of ordinary and reinforced stone columns. *Structures* **2020**, *25*, 481–490. [CrossRef]
34. Xin, T.; Minghua, Z.; Wei, C. Numerical Simulation of a Single Stone Column in Soft Clay Using the Discrete-Element Method. *Int. J. Geomech.* **2018**, *18*, 04018176. [CrossRef]
35. Hamzh, A.; Mohamad, H.; Bin Yusof, M.F. The effect of stone column geometry on soft soil bearing capacity. *Int. J. Geotech. Eng.* **2022**, *16*, 200–210. [CrossRef]
36. Abdellatief, M.; Mortagi, M. Predicting unconfined compressive strength of geopolymer-stabilized clays using a sector fruit fly–based extreme learning machine. *Sci. Rep.* **2026**, *16*, 12723. [CrossRef] [PubMed]
37. Abdellatief, M.; ElNemr, A.; Altahrany, A. Pareto-optimized stacked ensemble machine learning framework for predicting bearing capacity of driven piles from static load test data. *Sci. Rep.* **2026**, *16*, 11360. [CrossRef] [PubMed]
38. Luo, F.; Li, Y.; Yao, Y.; Zhang, G. Simplified Analysis Method of Stone Column Reinforced Foundations Based on Homogenization Technique. *Transp. Geotech.* **2025**, *53*, 101601. [CrossRef]

39. Gnananandarao, T.; Onyelowe, K.C.; Murthy, K.S.R. Experience in using sensitivity analysis and ANN for predicting the reinforced stone columns' bearing capacity sited in soft clays. In *Artificial Intelligence and Machine Learning in Smart City Planning*; Elsevier: Amsterdam, The Netherlands, 2023; pp. 231–241. [CrossRef]
40. Fattahi, H.; Ghaedi, H.; Malekmahmoodi, F.; Armaghani, D.J. Accurate estimation of bearing capacity of stone columns reinforced: An investigation of different optimization algorithms. *Structures* **2024**, *64*, 106519. [CrossRef]
41. Kazemzadeh, M.; Zad, A.; Yazdi, M. Railway Track Performance Over Geogrid-Encased Stone Columns Under High-Speed Train Loads: A Numerical and Machine Learning Approach. *Transp. Infrastruct. Geotechnol.* **2025**, *12*, 175. [CrossRef]
42. Jasim, O.H.; Khaleel, F.; Khaleel, D.; Fattah, M.Y.; Alfahad, A.A.; AbdUlameer, A.H.; Afan, H. Predicting the factor of safety in embankments improved by geogrid-encased stone columns using various neural network architectures. *Model. Earth Syst. Environ.* **2025**, *11*, 438. [CrossRef]
43. Das, M.; Dey, A.K. Prediction of Bearing Capacity of Stone Columns Underlying a Soil–Cement Bed Using Support Vector Regression Approach. *Indian Geotech. J.* **2025**, *55*, 1168–1183. [CrossRef]
44. Aljanabi, Q.A.; Chik, Z.; Allawi, M.F.; El-Shafie, A.H.; Ahmed, A.N.; El-Shafie, A. Support vector regression-based model for prediction of behavior stone column parameters in soft clay under highway embankment. *Neural Comput. Appl.* **2018**, *30*, 2459–2469. [CrossRef]
45. Wu, Y.; Sicard, B.; Gadsden, S.A. Physics-informed machine learning: A comprehensive review on applications in anomaly detection and condition monitoring. *Expert Syst. Appl.* **2024**, *255*, 124678. [CrossRef]
46. Abdellatief, M.; Elsafi, M.; Murali, G.; ElNemr, A. Comparative evaluation of hybrid machine learning models for predicting the strength of metakaolin-based geopolymer concrete enhanced with Gaussian noise augmentation. *J. Build. Eng.* **2025**, *111*, 113302. [CrossRef]
47. Abdellatief, M.; Abd-Elmaboud, M.E.; Mortagi, M.; Saqr, A.M. A convolutional neural network-based deep learning approach for predicting surface chloride concentration of concrete in marine tidal zones. *Sci. Rep.* **2025**, *15*, 27611. [CrossRef] [PubMed]
48. Mokhtari, M.; Kalantari, B. Soft Soil Stabilization using Stone Column—A Review. *Electron. J. Geotech. Eng.* **2012**, *17*, 1659–1666.
49. Deb, K. A mathematical model to study the soil arching effect in stone column-supported embankment resting on soft foundation soil. *Appl. Math. Model.* **2010**, *34*, 3871–3883. [CrossRef]
50. Farik, A.; Djabri, M.; Kaab, M.Z.; Bouaicha, A.; Aouadj, A. Prediction and Optimization of Bearing Capacity for Shallow Foundations on Geosynthetic-Reinforced Soil Using Response Surface Methodology and Finite Element Modeling. *Transp. Infrastruct. Geotechnol.* **2025**, *12*, 264. [CrossRef]
51. Page, M.J.; McKenzie, J.E.; Bossuyt, P.M.; Boutron, I.; Hoffmann, T.C.; Mulrow, C.D.; Shamseer, L.; Tetzlaff, J.M.; Akl, E.A.; Brennan, S.E. The PRISMA 2020 statement: An updated guideline for reporting systematic reviews. *BMJ* **2021**, *372*, n71. [CrossRef] [PubMed]
52. Jie, H.; Shu-Lin, Y. Simplified Method for Consolidation Rate of Stone Column Reinforced Foundations. *J. Geotech. Geoenviron. Eng.* **2001**, *127*, 597–603. [CrossRef]
53. Das, A.K.; Deb, K. Response of stone column-improved ground under c-ϕ soil embankment. *Soils Found.* **2019**, *59*, 617–632. [CrossRef]
54. Li, L.; Li, J.; Zhan, Z.; Gui, Y.; Liu, J. Experimental analysis of reinforcement methods for stone column foundations. *Soils Found.* **2025**, *65*, 101661. [CrossRef]
55. Pandey, B.K.; Rajesh, S.; Chandra, S. Performance of Soft Clay Reinforced with Encased Stone Column: A Systematic Review. *Int. J. Geosynth. Ground Eng.* **2022**, *8*, 40. [CrossRef]
56. Poon, B.; Chan, K. Stress concentration ratio and design method for stone columns using 2D FEA with equivalent strips. In *Proceedings of the 18th International Conference on Soil Mechanics and Geotechnical Engineering*; Presses des Ponts: Paris, France, 2013; pp. 2585–2588.
57. Xu, Z.; Zhang, L.; Peng, B.; Zhou, S. DEM-FDM numerical investigation on load transfer mechanism of GESC-supported embankment. *Comput. Geotech.* **2021**, *138*, 104321. [CrossRef]
58. Pivarc, J. Stone Columns-Determination of the soil improvement factor. *Slovak J. Civ. Eng.* **2011**, *19*, 17.
59. Balaam, N.P.; Booker, J.R. Analysis of rigid rafts supported by granular piles. *Int. J. Numer. Anal. Methods Geomech.* **1981**, *5*, 379–403. [CrossRef]
60. Ambily, A.P.; Gandhi, S.R. Behavior of Stone Columns Based on Experimental and FEM Analysis. *J. Geotech. Geoenviron. Eng.* **2007**, *133*, 405–415. [CrossRef]
61. Huang, J.; Han, J. Two-dimensional parametric study of geosynthetic-reinforced column-supported embankments by coupled hydraulic and mechanical modeling. *Comput. Geotech.* **2010**, *37*, 638–648. [CrossRef]
62. Yapage, N.N.S.; Liyanapathirana, D.S. A parametric study of geosynthetic-reinforced column-supported embankments. *Geosynth. Int.* **2014**, *21*, 213–232. [CrossRef]
63. Sudip, B.; Buddhima, I.; Cholachat, R.; Firman, S. Modeling the Stone Column Behavior in Soft Ground with Special Emphasis on Lateral Deformation. *J. Geotech. Geoenviron. Eng.* **2017**, *143*, 04017016. [CrossRef]

64. Castro, J.; Sagaseta, C. Consolidation around stone columns. Influence of column deformation. *Int. J. Numer. Anal. Methods Geomech.* **2009**, *33*, 851–877. [CrossRef]
65. Rathgeb, E.; Kutzner, C. Some applications of the vibro-replacement process. *Geotechnique* **1975**, *25*, 45–50. [CrossRef]
66. Zhang, L.; Xu, Z.; Zhou, S. Vertical cyclic loading response of geosynthetic-encased stone column in soft clay. *Geotext. Geomembr.* **2020**, *48*, 897–911. [CrossRef]
67. Tan, X.; Luo, M.; Yin, X.; Hu, Z.; Jin, Y.; Chen, C. Numerical Study of the Failure Process of Stone Column Groups in Soft Soil in Response to Rigid Loading Based on the DEM-FDM Coupled Model. *Int. J. Geomech.* **2025**, *25*, 04025032. [CrossRef]
68. Deb, K.; Dhar, A. Optimum design of stone column-improved soft soil using multiobjective optimization technique. *Comput. Geotech.* **2011**, *38*, 50–57. [CrossRef]
69. Tan, X.; Hu, Z.; Yin, X.; Chen, C.; Chen, J. Performance of geotextile-wrapped stone columns under uniaxial compression loading: Numerical simulation and analytical solution. *Constr. Build. Mater.* **2025**, *471*, 140663. [CrossRef]
70. Chen, J.F.; Li, L.Y.; Zhang, Z.; Zhang, X.; Xu, C.; Rajesh, S.; Feng, S.Z. Centrifuge modeling of geosynthetic-encased stone column-supported embankment over soft clay. *Geotext. Geomembr.* **2021**, *49*, 210–221. [CrossRef]
71. Tan, X.; Hu, Z.; Cao, M.; Chen, C. 3D discrete element simulation of a geotextile-encased stone column under uniaxial compression testing. *Comput. Geotech.* **2020**, *126*, 103769. [CrossRef]
72. Sun, J.; Lu, M.; Xu, B.; Shan, J. Consolidation of high replacement ratio stone column-reinforced ground: Analytical solutions incorporating clogging effect. *J. Rock Mech. Geotech. Eng.* **2024**, *16*, 3311–3326. [CrossRef]
73. Pal, S.; Deb, K. Effect of clogging of stone column on drainage capacity during soil liquefaction. *Soils Found.* **2019**, *59*, 196–207. [CrossRef]
74. Sudip, B.; Buddhima, I.; Cholachat, R. Modeling the Performance of Stone Column–Reinforced Soft Ground under Static and Cyclic Loads. *J. Geotech. Geoenviron. Eng.* **2016**, *142*, 04015067. [CrossRef]
75. Buddhima, I.; Sudip, B.; Cholachat, R. Numerical Solution of Stone Column–Improved Soft Soil Considering Arching, Clogging, and Smear Effects. *J. Geotech. Geoenviron. Eng.* **2013**, *139*, 377–394. [CrossRef]
76. Han, J.; Ye, S.L. A Theoretical Solution for Consolidation Rates of Stone Column-Reinforced Foundations Accounting for Smear and Well Resistance Effects. *Int. J. Geomech.* **2002**, *2*, 135–151. [CrossRef]
77. Castro, J.; Sagaseta, C. Deformation and consolidation around encased stone columns. *Geotext. Geomembr.* **2011**, *29*, 268–276. [CrossRef]
78. Miranda, M.; Fernández-Ruiz, J.; Castro, J. Critical length of encased stone columns. *Geotext. Geomembr.* **2021**, *49*, 1312–1323. [CrossRef]
79. Murugesan, S.; Rajagopal, K. Geosynthetic-encased stone columns: Numerical evaluation. *Geotext. Geomembr.* **2006**, *24*, 349–358. [CrossRef]
80. Kang, B.; Wang, J.; Zhou, Y.; Huang, S. Study on Bearing Capacity and Failure Mode of Multi-Layer-Encased Geosynthetic-Encased Stone Column under Dynamic and Static Loading. *Sustainability* **2023**, *15*, 5205. [CrossRef]
81. McCabe, B.A.; Killeen, M.M. Small Stone-Column Groups: Mechanisms of Deformation at Serviceability Limit State. *Int. J. Geomech.* **2017**, *17*, 04016114. [CrossRef]
82. Etezad, M.; Hanna, A.M.; Khalifa, M. Bearing Capacity of a Group of Stone Columns in Soft Soil Subjected to Local or Punching Shear Failures. *Int. J. Geomech.* **2018**, *18*, 04018169. [CrossRef]
83. Bouassida, M. Comprehensive design of columnar reinforced foundations. *Int. J. Geotech. Eng.* **2013**, *7*, 156–164. [CrossRef]
84. Naskar, S.; Gupta, S.K.; Choudhary, A.K.; Sharma, K.K. 3D Finite Element Analysis of Stone Column Behaviour in Layered Soil with Geosynthetic Reinforced Soil Beds. *Arab. J. Sci. Eng.* **2025**, *50*, 13385–13403. [CrossRef]
85. Barksdale, R.D.; Bachus, R.C.; Barksdale, R.D. *Design and Construction of Stone Columns*; US Department of Transportation, Federal Highway Administration: Washington, DC, USA, 1983.
86. Kim, B.-I.; Lee, S.-H. Comparison of bearing capacity characteristics of sand and gravel compaction pile treated ground. *KSCE J. Civ. Eng.* **2005**, *9*, 197–203. [CrossRef]
87. Hugher, J.M.O.; Withers, N.J. Reinforcing of soft cohesive soils with stone columns. *Ground Eng.* **1974**, *7*, 42–49.
88. Salam, M.A.; Wang, Q.; Huang, J. Experimental and numerical study on the composite column behavior: Loess soil reinforced by concrete-stone column. *Civ. Eng. J.* **2022**, *8*, 2022. [CrossRef]
89. Neeraj, K.; Rakesh, K. Performance of Geosynthetic-Encased Stone Columns in Sandy Soils Subjected to Vertical Cyclic Loads. *Int. J. Geomech.* **2025**, *25*, 04024323. [CrossRef]
90. Abid, M.S.; Rathod, D.; Vanapalli, S.K. 3-Dimensional numerical analysis of geosynthetic double-encased annulus stone columns. *Geosynth. Int.* **2024**, *32*, 579–597. [CrossRef]
91. Choobbasti, A.J.; Zahmatkesh, A.; Noorzad, R. Performance of Stone Columns in Soft Clay: Numerical Evaluation. *Geotech. Geol. Eng.* **2011**, *29*, 675–684. [CrossRef]
92. Al-Kazzaz, Z.A.; Al-Obaydi, M.A. Effect of spacing between stone columns on the behavior of soft soil. In *E3S Web of Conferences*; EDP Sciences: Les Ulis, France, 2021; p. 01006.

93. Negesa, A.B. Comparative analysis on effectiveness of crushed aggregate and scoria gravel as columnar reinforcement material under raft foundation. *Results Eng.* **2023**, *19*, 101254. [CrossRef]
94. Kahyaoğlu, M.R.; Doğan, T. Numerical study on the deformation behavior of geosynthetic-encased stone columns supporting embankments. *Tek. Dergi* **2022**, *33*, 12617–12634. [CrossRef]
95. Debbabi, I.E.; Saddek, R.M.; Rashid, A.S.A.; Muhammed, A.S. Numerical modeling of encased stone columns supporting embankments on sabkha soil. *Civ. Eng. J.* **2020**, *6*, 1593–1608. [CrossRef]
96. Shivashankar, R.; Babu, M.R.D.; Nayak, S.; Rajathkumar, V. Experimental Studies on Behaviour of Stone Columns in Layered Soils. *Geotech. Geol. Eng.* **2011**, *29*, 749–757. [CrossRef]
97. Al Ammari, K.; Clarke, B.G. Effect of Vibro Stone-Column Installation on the Performance of Reinforced Soil. *J. Geotech. Geoenviron. Eng.* **2018**, *144*, 04018056. [CrossRef]
98. Castro, J.; Karstunen, M.; Sivasithamparam, N. Influence of stone column installation on settlement reduction. *Comput. Geotech.* **2014**, *59*, 87–97. [CrossRef]
99. Ayub, F.; Khan, S.A. An overview of geopolymer composites for stabilization of soft soils. *Constr. Build. Mater.* **2023**, *404*, 133195. [CrossRef]
100. Deb, K.; Samadhiya, N.K.; Namdeo, J.B. Laboratory model studies on unreinforced and geogrid-reinforced sand bed over stone column-improved soft clay. *Geotext. Geomembr.* **2011**, *29*, 190–196. [CrossRef]
101. El Sawwaf, M.A. Behavior of strip footing on geogrid-reinforced sand over a soft clay slope. *Geotext. Geomembr.* **2007**, *25*, 50–60. [CrossRef]
102. Raithel, M.; Küster, V.; Lindmark, A. Geotextile-Encased Columns-a foundation system for earth structures, illustrated by a dyke project for a works extension in Hamburg. In *Nordic Geotechnical Meeting NGM*; Citeseer: University Park, PA, USA, 2004; pp. 1–10.
103. Mohamed, M.K.; Sakr, M.A.; Azzam, W.R. Geotechnical behavior of encased stone columns in soft clay soil. *Innov. Infrastruct. Solut.* **2023**, *8*, 80. [CrossRef]
104. Jamsawang, P.; Bergado, D.T.; Voottipruex, P.; Baez, F.; Jongpradist, P. A case study of the application of wet top-feed vibro replacement stone columns as foundation supports for a fuel tank in a reclamation area. *Bull. Eng. Geol. Environ.* **2024**, *84*, 4. [CrossRef]
105. Wang, Z.F.; Cheng, W.C. Predicting jet-grout column diameter to mitigate the environmental impact using an artificial intelligence algorithm. *Undergr. Space* **2021**, *6*, 267–280. [CrossRef]
106. Wang, Z.F.; Shen, S.L.; Modoni, G.; Zhou, A. Excess pore water pressure caused by the installation of jet grouting columns in clay. *Comput. Geotech.* **2020**, *125*, 103667. [CrossRef]
107. Borges, J.L.; Marques, D.O. Geosynthetic-reinforced and jet grout column-supported embankments on soft soils: Numerical analysis and parametric study. *Comput. Geotech.* **2011**, *38*, 883–896. [CrossRef]
108. Abd-Elhamed, A.; Mahmoud, S. Seismic response evaluation of structures on improved liquefiable soil. *Eur. J. Environ. Civ. Eng.* **2021**, *25*, 1695–1717. [CrossRef]
109. Serridge, C.J. Briefing: Dry bottom-feed stone column construction in soft fine-grained soils. *Proc. Inst. Civ. Eng.-Ground Improv.* **2015**, *168*, 159–161. [CrossRef]
110. Alnmr, A.; Ray, R.P.; Alsirawan, R. A State-of-the-Art Review and Numerical Study of Reinforced Expansive Soil with Granular Anchor Piles and Helical Piles. *Sustainability* **2023**, *15*, 2802. [CrossRef]
111. Raju, V.R.; Sondermann, W. Ground improvement using deep vibro techniques. In *Elsevier Geo-Engineering Book Series*; Elsevier: Amsterdam, The Netherlands, 2005; pp. 601–638.
112. Cai, G.; Liu, S.; Tong, L.; Du, G. Assessment of direct CPT and CPTU methods for predicting the ultimate bearing capacity of single piles. *Eng. Geol.* **2009**, *104*, 211–222. [CrossRef]
113. Golafzani, S.H.; Chenari, R.J.; Eslami, A. Reliability based assessment of axial pile bearing capacity: Static analysis, SPT and CPT-based methods. *Georisk Assess. Manag. Risk Eng. Syst. Geohazards* **2020**, *14*, 216–230. [CrossRef]
114. Gu, M.; Cai, X.; Qiu, J.; Zhang, X.; Han, D. Dynamic Behavior of Stone Column–Improved Soft Clay under Three-Stage Traffic Loads. *Int. J. Geomech.* **2025**, *25*, 04024322. [CrossRef]
115. Nujid, M.M.; Tholibon, D.A.; Mukhlisin, M. Numerical Simulation of Stone Column Performance Under Static and Cyclic Dynamic Loads in Multiple Soil Profiles with Diverse Rock Types. *Indian Geotech. J.* **2025**, *56*, 2008–2027. [CrossRef]
116. Liu, M.; Wang, K.; Niu, J.; Ouyang, F. Static and Dynamic Load Transfer Behaviors of the Composite Foundation Reinforced by the Geosynthetic-Encased Stone Column. *Sustainability* **2023**, *15*, 1108. [CrossRef]
117. Wood, D.M.; Hu, W.; Nash, D.F.T. Group effects in stone column foundations: Model tests. *Géotechnique* **2000**, *50*, 689–698. [CrossRef]
118. McKelvey, D.; Sivakumar, V.; Bell, A.; Graham, J. Modelling vibrated stone columns in soft clay. *Proc. Inst. Civ. Eng.-Geotech. Eng.* **2004**, *157*, 137–149. [CrossRef]

119. Black, J.A.; Sivakumar, V.; Bell, A. The settlement performance of stone column foundations. *Géotechnique* **2011**, *61*, 909–922. [CrossRef]
120. Alkhorshid, N.R.; Araujo, G.L.S.; Palmeira, E.M.; Zornberg, J.G. Large-scale load capacity tests on a geosynthetic encased column. *Geotext. Geomembr.* **2019**, *47*, 632–641. [CrossRef]
121. Priebe, H.J. Evaluation of the settlement reduction of a foundation improved by Vibro-Replacement. *Bautechnik* **1976**, *2*, 160–162.
122. Gäb, M.; Schweiger, H.F.; Kamrat-Pietraszewska, D.; Karstunen, M. Numerical analysis of a floating stone column foundation using different constitutive models. In *Geotechnics of Soft Soils: Focus on Ground Improvement*; CRC Press: Boca Raton, FL, USA, 2008; pp. 149–154.
123. Baumann, V.; Bauer, G.E.A. The performance of foundations on various soils stabilized by the vibro-compaction method. *Can. Geotech. J.* **1974**, *11*, 509–530. [CrossRef]
124. Nasiri, M.; Amiri, E.; Fadaei, E. Ensemble Machine Learning Models for Estimating Stone Column Load-Bearing Capacity Using Combined Experimental and Field Test Data. *Transp. Infrastruct. Geotechnol.* **2025**, *12*, 246. [CrossRef]
125. Zeini, H.A.; Lwti, N.K.; Imran, H.; Henedy, S.N.; Bernardo, L.F.A.; Al-Khafaji, Z. Prediction of the Bearing Capacity of Composite Grounds Made of Geogrid-Reinforced Sand over Encased Stone Columns Floating in Soft Soil Using a White-Box Machine Learning Model. *Appl. Sci.* **2023**, *13*, 5131. [CrossRef]
126. Kuo, Y.L.; Jaksa, M.B.; Lyamin, A.V.; Kaggwa, W.S. ANN-based model for predicting the bearing capacity of strip footing on multi-layered cohesive soil. *Comput. Geotech.* **2009**, *36*, 503–516. [CrossRef]
127. Momeni, E.; Nazir, R.; Armaghani, D.J.; Maizir, H. Prediction of pile bearing capacity using a hybrid genetic algorithm-based ANN. *Measurement* **2014**, *57*, 122–131. [CrossRef]
128. Chik, Z.; Aljanabi, Q.A. Intelligent prediction of settlement ratio for soft clay with stone columns using embankment improvement techniques. *Neural Comput. Appl.* **2014**, *25*, 73–82. [CrossRef]
129. Mosallanezhad, M.; Moayedi, H. Developing hybrid artificial neural network model for predicting uplift resistance of screw piles. *Arab. J. Geosci.* **2017**, *10*, 479. [CrossRef]
130. Sahu, R.; Patra, C.R.; Sivakugan, N.; Das, B.M. Bearing capacity prediction of inclined loaded strip footing on reinforced sand by ANN. In *International Congress and Exhibition" Sustainable Civil Infrastructures: Innovative Infrastructure Geotechnology"*; Springer: Berlin/Heidelberg, Germany, 2017; pp. 97–109.
131. Moayedi, H.; Rezaei, A. An artificial neural network approach for under-reamed piles subjected to uplift forces in dry sand. *Neural Comput. Appl.* **2019**, *31*, 327–336. [CrossRef]
132. Das, M.; Dey, A.K. Determination of bearing capacity of stone column with application of neuro-fuzzy system. *KSCE J. Civ. Eng.* **2018**, *22*, 1677–1683. [CrossRef]
133. Dey, A.K.; Debnath, P. Empirical approach for bearing capacity prediction of geogrid-reinforced sand over vertically encased stone columns floating in soft clay using support vector regression. *Neural Comput. Appl.* **2020**, *32*, 6055–6074.
134. Mazumder, T.; Garg, A. *Comparison of Accuracy in Prediction of Radial Strain in Stone Columns Using AI Based Models*; Belt and Road Webinar Series on Geotechnics, Energy and Environment; Springer: Singapore, 2021; pp. 209–222.
135. Moayedi, H.; Hayati, S. Applicability of a CPT-based neural network solution in predicting load-settlement responses of bored pile. *Int. J. Geomech.* **2018**, *18*, 06018009. [CrossRef]
136. Armaghani, D.J.; Shoib, R.S.N.S.B.R.; Faizi, K.; Rashid, A.S.A. Developing a hybrid PSO–ANN model for estimating the ultimate bearing capacity of rock-socketed piles. *Neural Comput. Appl.* **2017**, *28*, 391–405. [CrossRef]
137. Bagińska, M.; Srokosz, P.E. The optimal ANN Model for predicting bearing capacity of shallow foundations trained on scarce data. *KSCE J. Civ. Eng.* **2019**, *23*, 130–137. [CrossRef]
138. Sethy, B.P.; Patra, C.; Das, B.M.; Sobhan, K. Prediction of ultimate bearing capacity of circular foundation on sand layer of limited thickness using artificial neural network. *Int. J. Geotech. Eng.* **2021**, *15*, 1252–1267.
139. Ardakani, A.; Dinarvand, R.; Namaei, A. Ultimate shear resistance of silty sands improved by stone columns estimation using neural network and imperialist competitive algorithm. *Geotech. Geol. Eng.* **2020**, *38*, 1485–1496.
140. Ghanizadeh, A.R.; Ghanizadeh, A.; Asteris, P.G.; Fakharian, P.; Armaghani, D.J. Developing bearing capacity model for geogrid-reinforced stone columns improved soft clay utilizing MARS-EBS hybrid method. *Transp. Geotech.* **2023**, *38*, 100906. [CrossRef]
141. Lafifi, B.; Rouaiguia, A.; Soltani, E.A. A novel method for optimizing parameters influencing the bearing capacity of geosynthetic reinforced sand using RSM, ANN, and multi-objective genetic algorithm. *Stud. Geotech. Mech.* **2023**, *45*, 174–196. [CrossRef]
142. Foda, T.; Hassan, H.M.; Abdelkader, A.; el-Hassan, K.A. Predictive modeling of sustainable recycled materials for stone column construction. *Innov. Infrastruct. Solut.* **2024**, *9*, 408. [CrossRef]
143. Nivedhitha, R.; Bhasi, A.; Davis, R. Machine Learning Approaches for the Prediction of Bearing Capacity of Ordinary Stone Columns. In *Proceedings of the Indian Geotechnical Conference (IGC 2024)*; Dixit, M.S., Jaiswal, S.S., Shermale, Y., Singh, A.P., Maji, V.B., Eds.; Springer Nature: Singapore, 2025; Volume 8, pp. 155–165.
144. Meethal, R.E.; Kodakkal, A.; Khalil, M.; Ghantasala, A.; Obst, B.; Bletzinger, K.-U.; Wüchner, R. Finite element method-enhanced neural network for forward and inverse problems. *Adv. Model. Simul. Eng. Sci.* **2023**, *10*, 6. [CrossRef]

145. Abdellatief, M.; Baktheer, A.; Shahin, M.; Abadel, A.A.; Heniegal, A.M. Production and optimization of affordable artificial geopolymer aggregates containing crumb rubber, plastic waste, and granulated cork based on machine learning algorithms. *Case Stud. Constr. Mater.* **2025**, *22*, e04725. [CrossRef]
146. Abdellatief, M.; Hassan, Y.M.; Elnabwy, M.T.; Wong, L.S.; Chin, R.J.; Mo, K.H. Investigation of machine learning models in predicting compressive strength for ultra-high-performance geopolymer concrete: A comparative study. *Constr. Build. Mater.* **2024**, *436*, 136884. [CrossRef]
147. Abdellatief, M.; Wong, L.S.; Din, N.M.; Mo, K.H.; Ahmed, A.N.; El-Shafie, A. Evaluating enhanced predictive modeling of foam concrete compressive strength using artificial intelligence algorithms. *Mater. Today Commun.* **2024**, *40*, 110022. [CrossRef]
148. International Organization for Standardization. *Environmental Management: Life Cycle Assessment; Principles and Framework*; ISO: Geneva, Switzerland, 2006.